Differential cross section measurements for hadron therapy: 50 MeV/nucleon ^{12}C reactions on H, C, O, Al, and ^{nat}Ti targets

C. Divay,[1,*] J. Colin,[1] D. Cussol,[1] Ch. Finck,[2] Y. Karakaya,[2] M. Labalme,[1] M. Rousseau,[2] S. Salvador,[1] and M. Vanstalle[2]

[1]*LPC Caen, ENSICAEN, Université de Caen Normandie, CNRS/IN2P3, Caen, France*
[2]*Institut Pluridisciplinaire Hubert Curien, Strasbourg, France*

During a carbon therapy treatment, the beam undergoes inelastic nuclear reactions leading to the production of secondary fragments. These nuclear interactions tend to delocate a part of the dose into healthy tissues and create a mixed radiation field. In order to accurately estimate the dose deposited into the tissues, the production rate of these fragments all along the beam path have to be taken into account. But the double differential carbon fragmentation cross sections are not well known in the energy range needed for a treatment (up to 400 MeV/nucleon). Therefore, a series of experiments aiming to measure the double differential fragmentation cross sections of carbon on thin targets of medical interest has been started by our collaboration. In March 2015 we performed an experiment to study the fragmentation of a 50 MeV/nucleon ^{12}C beam on thin targets at GANIL. During this experiment, energy and angular cross-section distributions on H, C, O, Al, and ^{nat}Ti have been measured. The experimental set-up will be detailed as well as the systematic error study and all the experimental results will be presented.

I. INTRODUCTION

The use of carbon ions in hadron therapy is mostly motivated by two benefits. The higher mass of carbon ions compared to protons reduces lateral scattering, leading to a better control of the dose deposition [1]. But what appoints ^{12}C ions as one of the most suitable candidates to treat radioresistant tumors is that its relative biological effectiveness (RBE) reaches a maximum in the Bragg peak region 2 to 3 times higher than for protons or photons [1]. These advantages lead to increase damages for a given physical dose at the tumor location, while reducing the damages to the surrounding healthy tissues.

However, accelerated ions going through matter are subject to nuclear reactions, which have for a first consequence to reduce the beam intensity along the penetration path [2]. For instance, only 50% of the primary ions reach the Bragg peak position at 16 cm depth in water [3,8]. Moreover, secondary fragments created by these reactions lead to a delocalization of the dose in the surrounding healthy tissues and to a mixed irradiation field of heterogeneous RBE values that will modify the biological dose distribution. These effects must be taken into account in treatment planning systems (TPS) to accurately evaluate the appropriate dose delivery for a tumor treatment. The production rate of secondary particles, their angular and energy distributions are not well known up to the maximum beam energy of a treatment (i.e., 400 MeV/nucleon). However, nuclear models included in the simulation codes used to compute the transportation of ions through matter are unable to provide accurate fragmentation cross sections in the whole energy range [4–7].

Several years ago, a series of ^{12}C fragmentation measurements started to provide such data. First, measurements on thick tissue equivalent targets (PMMA and water) were performed at the Heavy Ion Medical Accelerator in Chiba (HIMAC), Japan [8–10] and at the GSI Helmholtz Centre for Heavy Ion Research in Germany [3,11–14]. These experiments have provided integrated flux and energy distributions measurements of the secondary fragments for beam energies between 200 and 400 MeV/nucleon. In 2008, our collaboration conducted an experiment to measure the angular and energy distributions of the fragments produced by nuclear reactions of a 95 MeV/nucleon ^{12}C beam on thick (up to 25 mm) PMMA targets [15]. This last experiment has shown that integrated measurements hardly constrain reaction models. Since, fragmentation cross sections measurements are performed using thin targets ($<$500 μm). A 62 MeV/nucleon ^{12}C experiment on a carbon target was performed at LNS in Catania [4]. Two experiments with 95 MeV/nucleon ^{12}C beams were performed by our collaboration in 2011 [16] and 2013 [17] at the Grand Accélérateur National d'Ions Lourds (GANIL) in Caen to measure the energy and angular differential fragmentation cross sections on thin targets of medical interest (H, C, Al, O, and ^{nat}Ti). The data from this experiment are currently used to constrain the new versions of nuclear models such as JQMD [18] in the Monte Carlo particle transport simulation code PHITS [19], LAQGSM [20] in MCNP6 [21], and INCL++ [22] in GEANT4 [23]. In March 2015, a new experiment with a 50 MeV/nucleon ^{12}C beam on the same targets has been conducted at GANIL to extract fragmentation cross sections on the last centimeter of the ion range. Indeed, this region is mainly located within the tumor where the maximum dose is deposited through the Bragg peak and is usually surrounded by organs at risk. These data will provide improved knowledge on fragmentation cross sections for increased precision on the dose calculation

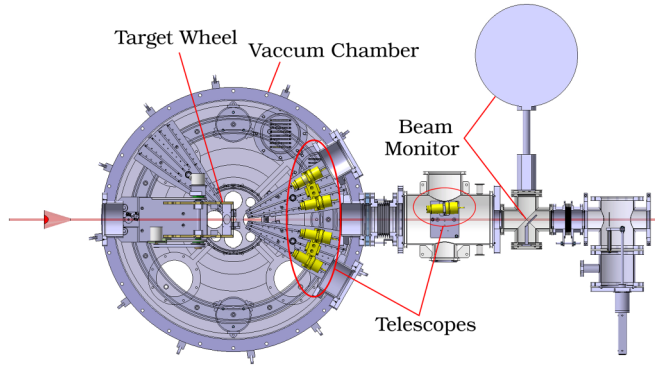*Corresponding author: divay@lpccaen.in2p3.fr

FIG. 1. A global view of the experimental set-up. The telescopes on their rotating supports, the beam monitor as well as the target wheel are represented.

as well as constraints to existing or new nuclear interaction models.

In this paper, the results of this last experiment will be presented. The experimental setup will be detailed and the data analysis and systematic error estimation will be presented. Finally, the results will be displayed, discussed, and compared to a previous experiment.

II. EXPERIMENTAL SETUP

The experiment took place on the GANIL G2 line with a 50.13 MeV/nucleon ^{12}C beam. Targets and detectors were confined in a vacuum reaction chamber. As the human body is composed of over 95% of four elementary elements, C, H, O, and Ca, double differential fragmentation cross sections on thin targets composed of these elements have to be measured. For H and O, composite targets were used: coupling CH_2 with C allows the calculation of the cross sections for H (see Sec. V). In the same way, Al_2O_3 and Al targets were used to calculate the oxygen cross sections. Due to difficulties to manufacture and handle a calcium target, we opted for a titanium target instead. We assumed that the measured cross sections for ^{nat}Ti would be very close to those of ^{40}Ca as our experimental set-up was mostly sensitive to the fragmentation of the projectile. All targets were mounted on a rotating wheel, visible in Fig. 1. Their thicknesses as well as their area densities (and their relative errors) are gathered in Table I.

TABLE I. Target thickness (in μm), area density ρ th (in g cm^{-2}) and its relative error $\sigma_{\rho\,th}/\rho$ th.

Targets	Thickness (μm)	ρ th (g cm^{-2})	$\sigma_{\rho\,th/\rho\,th}$ (%)
C	250	0.043	0.46
CH_2	400	0.037	0.56
Ti	100	0.048	0.22
Al	150	0.040	0.25
Al_2O_3	150	0.050	0.07
PMMA	500	0.064	0.80

The detection setup consisted of five telescopes, each composed of three layers: a thin silicon diode ($\sim$150 μm thick), a thick silicon diode ($\sim$500 μm thick), and a conical CsI:Tl scintillating crystal of 75 mm long and 1 μs decay constant coupled to a photomultiplier tube (PMT). Both diodes had a diameter of 22 mm. The entrance diameter of the CsI was 25 mm and grew up to 28 mm. The conical shape was chosen to prevent a maximum of particles from escaping from the sides of the detector. This calorimeter was held in an aluminum frame and was separated from the thick silicon layer by a 2.5 μm thick aluminized mylar foil.

One telescope was fixed at a 3° angle and 81.36 cm behind the target, covering a solid angle of 0.45 msr. The other four telescopes were positioned on rotating supports to cover angles ranging from 5° to 39°. They were located 28.75 cm behind the target, each covering a solid angle of 3.67 msr.

In order to measure the ion beam intensity, a silver foil of 7 μm thick was set in-beam after the detectors. The x rays emitted by the beam crossing the foil were measured by a Si(Li) detector. Their number, proportional to the number of incident ions, allowed us to measure the beam intensity. The calibration of the Si(Li) was done prior the experiment using a plastic scintillator located in beam read out by a PMT counting the number of impinging ions. During a cross section measurement, the beam intensity was not corrected by the number of beam particles fragmenting in the target as their proportion (less than 0.1%) was negligible compared to the error bar on the measured intensity. A detailed description of this calibration process can be found in [24]. The five telescopes as well as the beam monitor can be seen on Fig. 1.

Each detector was read by an in-house built digital acquisition system named FASTER [25]. The silicon diodes were connected to a 14 bits amplitude-to-digital converters inputs after being preamplified while the CsI detectors were connected to charge integrating inputs with three different time windows allowing for a pulse shape analysis of the signal.

III. DATA ANALYSIS

A. Identification process

The data analysis was achieved in the following way. The energy deposited in the thin Si detector was plotted as a function of the energy deposited in the thick Si detector to obtain a so-called ΔE-ΔE map. The energy deposited in the thick silicon diode was plotted versus the remaining energy in the CsI crystal to obtain a second ΔE-E map. Using the KaliVeda toolkit developed by the INDRA collaboration [26], parametric functions were used to fit both plots to perform particle identification and detector energy calibration at the same time (see, for example, Fig. 2). Moreover, using the different integration time windows on the CsI scintillation signal, one can achieve pulse shape analysis (PSA). By representing the "fast" component of the signal (the shortest time window consisting of the first 500 ns of the signal) versus the "slow" component (the time window of 3 μs), the charge and mass of the different isotopes can be separated (Fig. 3) and used as a complementary identification process. A
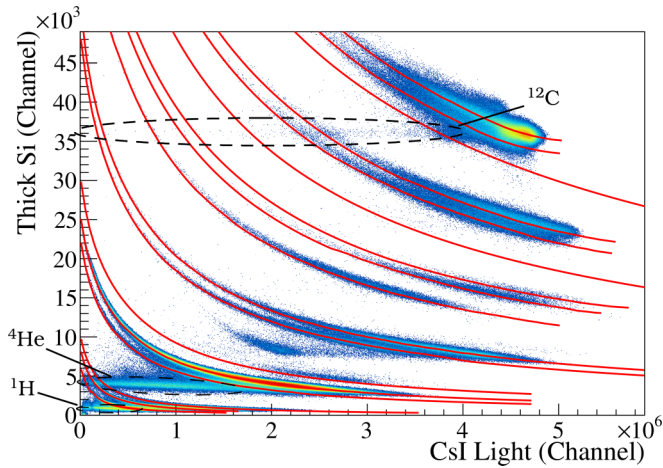
FIG. 2. ΔE-E map (thick silicon diode vs. CsI) with a KaliVeda identification grid (red lines). Dashed circles are displayed to highlight the horizontal trails coming from the proton, α, and ^{12}C lines caused by in-detector fragmentation or by particles escaping from the sides of the detector.

more detailed description of the analysis process can be found in [24].

B. Cleaning of the identification maps

Using only the ΔE-E identification method can introduce misidentifications. Nuclear reactions within the CsI as well as the escape of particles from the sides of the detector create horizontal trails on the ΔE-E maps. These "fragmentation trails," mostly visible for protons, ^{4}He, and ^{12}C (Fig. 2), crossed the other isotope lines and therefore polluted the other identification lines.

Moreover, the lines within a group of charge Z were not clearly separated at high CsI energy and isotopes can then be misidentified as belonging to one of the neighboring lines.
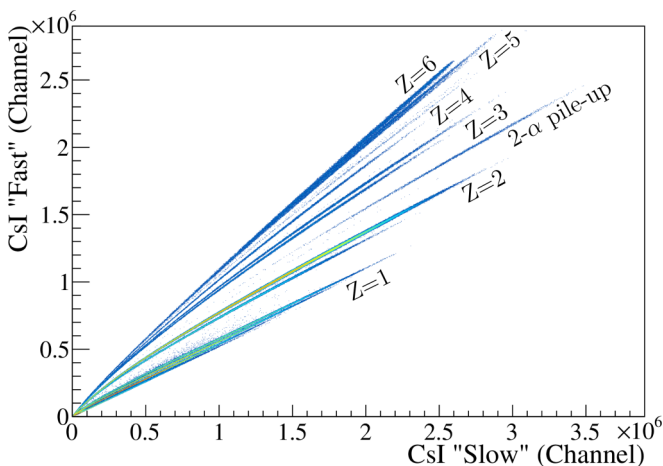

FIG. 3. Pulse shape analysis plot. The different isotopes are distributed along different lines and are clearly discernible for fragments with a charge below 5. The two α pile-up is clearly visible on a separate line.
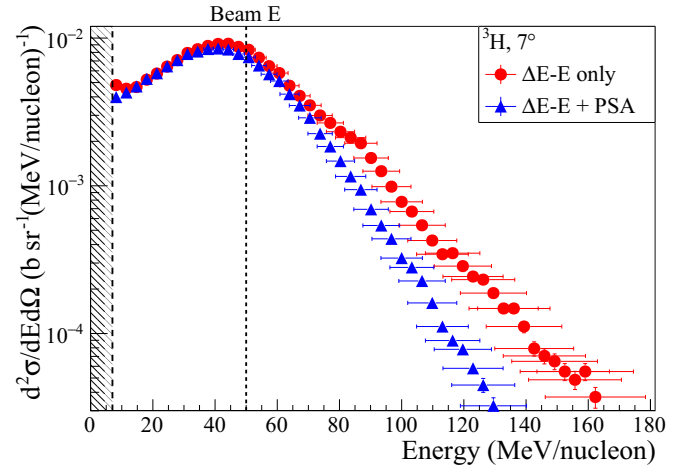

FIG. 4. Example of the misidentification effects on a ^{3}H energy distribution at $7°$. The distribution with red circles is the result of the KaliVeda identification and the one with blue triangles is the distribution corrected using the pulse shape analysis technique. The dotted line indicates the beam energy and the crosshatched area represents the energy threshold.

This was corrected using the pulse shape analysis after the KaliVeda identification process. By displaying the PSA plot for a single isotope, it was possible to recover misidentified events with graphical cuts, as the different isotopes appeared on separate lines. This was possible only for fragments with a charge below 5 as for higher charges values, the different masses were not distinguishable anymore on the PSA plot (see Fig. 3). An example of this correction is shown on Fig. 4 for ^{3}H. Two energy distributions are plotted: the primary identification is displayed as full circles (ΔE-E only) and the corrected distribution as triangles (ΔE-E + PSA). The low energy part of the two distributions are very similar. The discrepancies grow larger above 60 MeV/nucleon, where the non-corrected distribution shows some uneven structures while the corrected distribution shows a smooth slope. The importance of this correction varies greatly with the abundance of the isotope. For ^{3}H at $7°$ (Fig. 4), the proportion of the correction was 12.4% of the initial angular differential cross section. It is negligible for profuse isotopes such as protons ($\sim$1%) or ^{4}He ($\sim$4%), but the misidentification can sometimes predominate for scarce isotopes located next to abundant ones (e.g., up to 75% for ^{6}He). As for the parts of the "fragmentation trails" that are in-between isotope lines and too far from an identification line to be identified, they were recovered using graphical cuts over the data in the ΔE-E map. For the ^{12}C trail crossing the isotopes lines above ^{7}Be, it was not possible to separate the isotopes in the PSA plot, so the pollution induced by these trails was taken into account in the systematic errors study (see Sec. IV B).

Another main source of misidentification was the two α particles pile-up. Most of these events can be attributed to the disintegration of ^{8}Be into two α particles (with a half-life of 6.7×10^{-17} s). Due to quenching effect in the CsI scintillator, this 2α contribution was located in the same area as the lithium isotopes on the ΔE-E map. They contributed to 43.6% of

TABLE II. Energy thresholds in MeV/nucleon for the most produced isotope of each charge.

Isotope	^{1}H	^{4}He	^{6}Li
E_{th} (MeV/nucleon)	9.6	9.6	11.9
Isotope	^{7}Be	^{10}B	^{11}C
E_{th} (MeV/nucleon)	15.2	16.3	18.9

TABLE III. Systematic errors (ε_{Rel}) for several isotopes and three different angles. Estimated from Monte Carlo simulations.

Isotope	5°	15°	31°
p	0.14%	0.04%	1.29%
^{4}He	3.77%	4.53%	1.38%
^{6}Li	0.12%	1.20%	2.91%
^{9}Be	19.1%	13.5%	32.3%
^{10}B	10.6%	21.8%	–
^{11}C	3.70%	1.94%	–

the ^{7}Li amount and 12.1% of the total α amount at 5°. This proportion decreased with the angle (23.4% at 11° and 3.4% at 23° for lithium and 4.3% at 11° and 0.4% at 23° for α particles). In order to retrieve most of these events, which would otherwise participate in the systematic error estimation [24], we used the PSA plots. As seen in Fig. 3, these events grew on a clearly distinct line. They could therefore be flagged as α particles prior to the KaliVeda identification.

C. Energy computation

To measure the total energy of each detected particle, we extrapolated it from its deposited energy in the thick silicon diode. Once the particle is identified, its residual energy can be calculated using energy loss look-up tables. The total energy of the particle is then the sum of the energy deposited in the diodes and the calculated residual energy. The principal advantage of this method is to prevent from calibrating the nonlinear light response of the CsI calorimeter due to quenching effects [24].

Using the same process, we established the experimental energy thresholds for all detected particles. They are gathered in Table II for the most produced isotope of each charge and are represented by crosshatched areas on each figure displaying an energy distribution.

IV. SYSTEMATIC STUDY

A. Monte Carlo simulation of the experiment

In order to estimate the systematic errors of the data analysis process, a simulation of the experiment was done using the GEANT4 (v4.10-p02) simulation toolkit [23]. The quantum molecular dynamics (QMD) model [27] was chosen due to its ability to reproduce best the data we obtained in our 95 MeV/nucleon experiment [16]. The detectors geometry and their frames were reproduced and a parallel 50 MeV/nucleon ^{12}C beam with a gaussian profile of $\sigma = 2$ mm was used to reproduce the experimental beam shape.

For each event, a list of the particles that hit the telescopes featuring their name, charge, mass and individual energy deposition was recovered. The ΔE-E maps were also displayed. The data were analyzed using the KaliVeda tools in the same way as for the experimental data. In the end, the number of each isotope identified by our experimental analysis process ($N_{\text{Identified}}$) was compared to the amount of this isotope impinging the detector ($N_{\text{Impinging}}$). The relative error (ε_{Rel}) for each isotope and angle was determined using the following formula:

$$\varepsilon_{\text{Rel}}\left(^{A}_{Z}X\right) = 100\left(\frac{N_{\text{Identified}}\left(^{A}_{Z}X\right)}{N_{\text{Impinging}}\left(^{A}_{Z}X\right)} - 1\right), \quad (1)$$

where ε_{Rel} is the estimation of the error induced by our identification process, $N_{\text{Identified}}\left(^{A}_{Z}X\right)$ and $N_{\text{Impinging}}\left(^{A}_{Z}X\right)$ are the amount of $^{A}_{Z}X$ identified and impinging a detector, respectively.

The pulse shape analysis was not reproduced due to insufficient modelization of the crystal scintillation process. For this reason, the two α pile-up events which were corrected experimentally were removed from the lithium distributions in the simulation data. In the same way, the events from the ^{12}C trail were removed from the distributions of isotopes above lithium. Indeed, the nuclear models used could not replicate the production of beryllium and boron isotopes in a realistic way and they would be overwhelmed by the ^{12}C events. Even so, the low production rate of these isotopes in the simulation lead to high systematic errors (see Table III). This method allowed the evaluation of systematic errors induced by any kind of pile-up of particles and other pollution in the ΔE-E maps that were not correctible with our analysis. Some results of this simulation (ε_{Rel}) are gathered in Table III, for several isotopes and three different angles.

B. Experimental estimation of the error caused by the ^{12}C trail

As mentioned in Sec. III B, the events from the ^{12}C trail could not be recovered using the PSA method. However, as seen above, using the simulation to determine the proportion of ^{12}C in those isotopes would have led to a great overestimation. Hence, the choice was made to use an experimental method to estimate these errors. On the ΔE-E map, we graphically selected the areas polluted by the carbon trail for each isotope. The relative systematic error was then calculated using the formula:

$$\varepsilon_{\text{Trail}}\left(^{A}_{Z}X\right) = \frac{N_{\text{Selected}}\left(^{A}_{Z}X\right)}{N_{\text{Isotope}}\left(^{A}_{Z}X\right)}, \quad (2)$$

where $N_{\text{Selected}}\left(^{A}_{Z}X\right)$ is the number of events graphically selected on the $^{A}_{Z}X$ isotope line and $N_{\text{Isotope}}\left(^{A}_{Z}X\right)$ is the total amount of fragments of charge Z and mass A identified.

The total relative error is then calculated using the linear sum of all error sources, maximizing the error correlations:

$$\varepsilon_{\text{Tot}}\left(^{A}_{Z}X\right) = \varepsilon_{\text{Stat}}\left(^{A}_{Z}X\right) + \varepsilon_{\text{Rel}}\left(^{A}_{Z}X\right) + \varepsilon_{\text{Trail}}\left(^{A}_{Z}X\right), \quad (3)$$
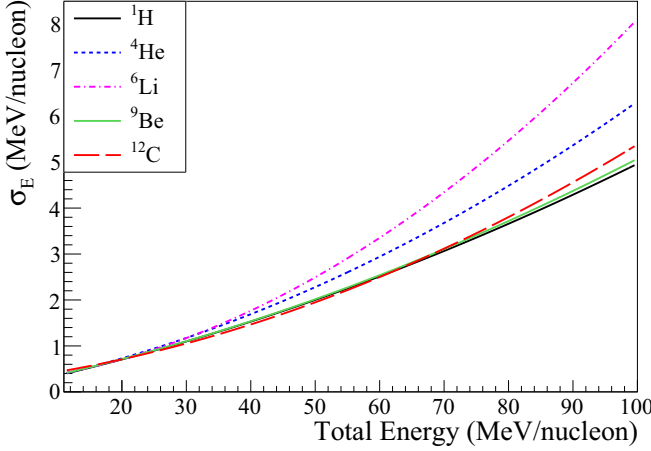
FIG. 5. Relation between the value of the total reconstructed energy and its uncertainty for several isotopes.

FIG. 6. ^{4}He measured cross sections for C (blue squares) and CH$_2$ (red circles) targets and calculated cross sections for H target (hollow black circles).

where $\varepsilon_{\mathrm{Stat}}$ is the relative statistical error for the isotope, $\varepsilon_{\mathrm{Rel}}$ is the systematic error estimated using the Monte Carlo simulation, and $\varepsilon_{\mathrm{Trail}}$ is the systematic error induced by the ^{12}C trail for lighter isotopes. This last term is nonzero for isotopes above lithium only.

C. Systematic error on the energy reconstruction

The error estimation on the reconstructed energy depends on the energy resolution of the thick silicon layer and on the amount of energy deposited by the particle. The total energy calculation is then less accurate for small values of deposited energy (e.g., high kinetic energy particles), as a small variation can lead to a large difference in reconstructed energy (up to $\sim$14% for 250 MeV protons). The energy resolution of each silicon diode was measured using a ^{241}Am source emitting mainly 5.486 MeV α particles. The measured energy resolutions range from 0.34% to 0.96%. Then, an error propagation method was used to estimate the variation of the calculated energy based on the energy resolution of the diode. This was done on a large energy range for each isotope and each telescope. Figure 5 shows the evolution of the uncertainty σ_E with the total reconstructed energy for one telescope and various isotopes.

V. RESULTS

The angular cross sections are calculated using the formula:

$$\frac{d\sigma}{d\Omega}\left(^A_Z X\right) = \frac{N\left(^A_Z X\right)}{N(^{12}\mathrm{C})} \frac{1}{\Omega} \frac{A_{\mathrm{target}}}{(\rho\,\mathrm{th})_{\mathrm{target}} \mathcal{N}_A}, \qquad (4)$$

where $N(^A_Z X)$ is the number of fragments of mass A and charge Z detected, $N(^{12}\mathrm{C})$ is the number of beam ions measured by the beam monitor, A_{target} is the number of mass of the target, Ω is the solid angle covered by the detector, $(\rho\,\mathrm{th})_{\mathrm{target}}$ is the area density of the target, and $\mathcal{N}_A$ is the Avogadro number.

As mentioned in Sec. II, composite targets were used to extract the cross sections for hydrogen and oxygen [16]. For both elemental targets, the following basic decomposition was used:
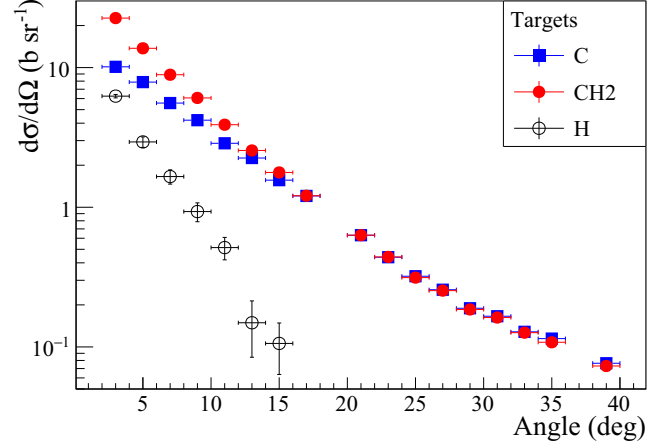
$$\frac{d\sigma}{d\Omega}(\mathrm{H}) = \frac{1}{2}\left(\frac{d\sigma}{d\Omega}(\mathrm{CH}_2) - \frac{d\sigma}{d\Omega}(\mathrm{C})\right),$$

$$\frac{d\sigma}{d\Omega}(\mathrm{O}) = \frac{1}{3}\left(\frac{d\sigma}{d\Omega}(\mathrm{Al}_2\mathrm{O}_3) - 2\frac{d\sigma}{d\Omega}(\mathrm{Al})\right). \qquad (5)$$

Figure 6 shows an example of the measured ^{4}He angular cross sections for C and CH$_2$ targets and the calculated angular cross sections for H target.

All angular and energy differential cross sections have been measured for every isotopes from proton to ^{12}C and every targets used in this experiment. The results are shown in full details in the Appendices (cf. Tables IV to VIII). In the following sections, the angular distributions, the energy distributions as well as the reconstruction of the cross sections for a PMMA target will be successively presented.

A. Angular distributions

Figure 7 shows an example of angular distributions obtained for the carbon target and various isotopes from ^{1}H to ^{10}C. A clear dominance of light isotopes (mostly protons and α particles) is observed over the whole angular range. The ^{4}He production dominates the proton production up to more than $20°$. The proton cross sections only slightly decrease from $3°$ to $39°$, resulting in a rather broad angular distribution. Overall, it can be seen that the higher the mass of the fragment, the more forward peaked the angular distribution. A comparison of cross sections for ^{4}He over all elemental targets (H, C, O, Al, Ti) is shown in Fig. 8. It is clear that the production cross sections increase with the mass of the target, especially at large angles. The distributions distinctly separate for angles above $20°$, where the midrapidity and quasitarget contribution takes over the quasi-projectile emission [28]. The shape with the hydrogen target is clearly distinct from the ones obtained with the other targets. The cross sections fall very quickly and are close to zero for angles higher than $15°$. This behavior is seen for all isotopes heavier than ^{3}He, as it has been
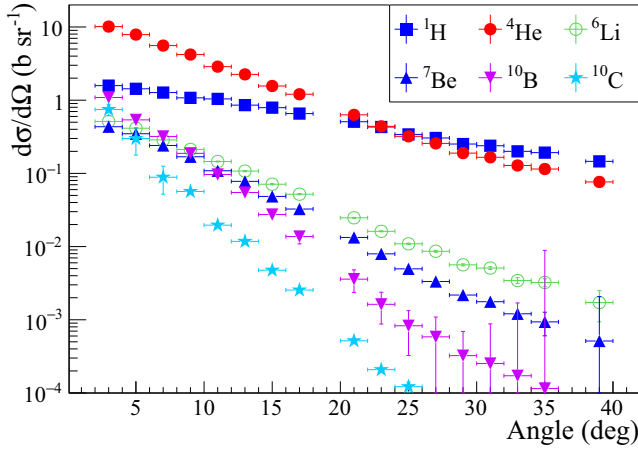
FIG. 7. Angular differential cross sections distributions of six isotopes from $Z = 1$ to $Z = 6$ for the carbon target.

observed in the previous experiment [28]. Indeed, there is no midrapidity emission of heavier fragments, as they are necessarily produced by the quasiprojectile.

B. Energy distributions

Energy distributions for ^{4}He particles and four different angles are shown in Fig. 9. At low angles, the distributions are peaked at slightly less than the beam energy. This peak then shifts to lower energies when the angle of emission increases. For higher angles, the peak disappears, confirming the fact that fragments from the quasiprojectile are primarily emitted at small angles and at energies close to the beam energy. They are less and less present at higher angles, where the midrapidity and the quasitarget emissions become dominant [28].

The cross sections slightly increase with the mass of the target, as shown in Fig. 10 for ^{4}He production. It is also seen that the heavier the target, the higher the cross sections at low energies. The hydrogen target distribution present a lack of low energy contribution. This might be due to the absence of

FIG. 9. Energy distributions for ^{4}He and four angles from $5°$ to $31°$ for the carbon target. The dotted line indicates the beam energy and the crosshatched area represents the energy threshold.

midrapidity and quasitarget emission for fragments with mass over 3.

C. PMMA cross sections reconstruction

Using the cross sections from each elemental target, we can compute the cross sections for composite materials. In this experiment, we used a $500 \, \mu$m thick PMMA target to test the accuracy of the cross sections reconstruction.

The cross section values have been calculated using the PMMA material chemical composition, $C_5H_8O_2$, with the following expression:

$$\frac{d\sigma}{d\Omega}(C_5H_8O_2) = 5\frac{d\sigma}{d\Omega}(C) + 8\frac{d\sigma}{d\Omega}(H) + 2\frac{d\sigma}{d\Omega}(O). \quad (6)$$

Comparisons between measured and calculated PMMA angular and energy distributions are displayed in Fig. 11(a) and 11(b), respectively. The data for $9°$, $15°$, $27°$, and $33°$ were
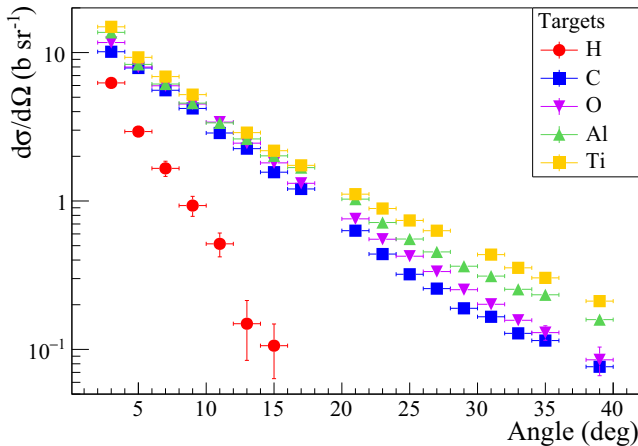

FIG. 8. Angular differential cross sections of ^{4}He for all elemental targets.

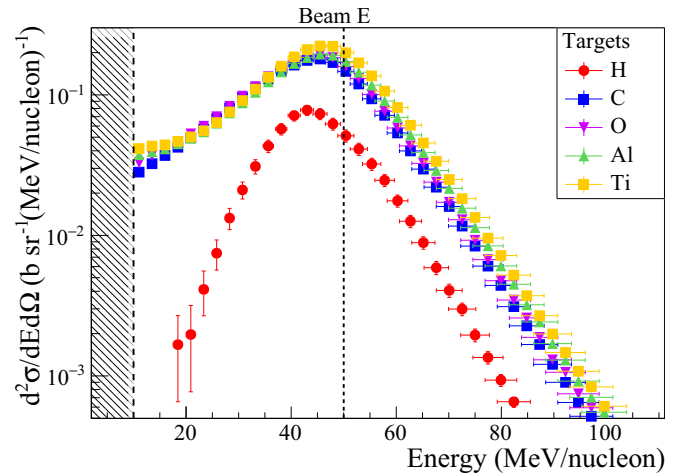FIG. 10. Energy distributions for ^{4}He and all elemental targets at $7°$. The dotted line indicates the beam energy and the crosshatched area represents the energy threshold.
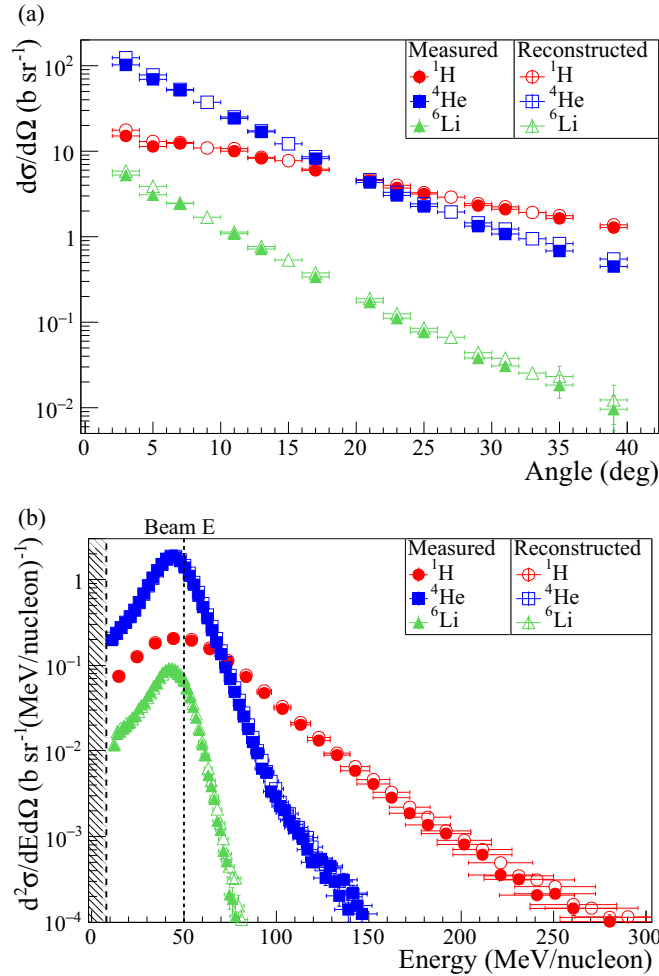
(a)

(b)

FIG. 11. Comparison between the measured (full dots) and reconstructed (hollow dots) PMMA angular and energy cross sections (up and down, respectively). The results are displayed for protons (red circles), ^{4}He (blue squares), and ^{6}Li (green triangles). The dotted line indicates the beam energy and the crosshatched area represents the energy threshold.

not measured for the PMMA target. The angular distributions for ^{1}H, ^{4}He, and ^{6}Li both measured and calculated are shown and are in good agreement. The energy distributions for the three same isotopes are compared for the 7° measurements in Fig. 11(b) and show an excellent agreement as well. The discrepancies for all isotopes are usually beneath a factor of 2, except for high angles, where the uncertainties on the measurements grow higher.

D. Data analysis validation

Figure 12 shows a comparison of the angular cross sections distributions from 3° to 22° of ^{4}He, ^{6}Li, and ^{9}Be isotopes with the data measured at LNS with a 62 MeV/nucleon ^{12}C beam on carbon target [4]. We can see that the distributions are matching in shape and absolute values, with discrepancies under a factor of 2 and within the error bars. This confirms the quality of the data analysis of the present work considering the very small observed discrepancies.
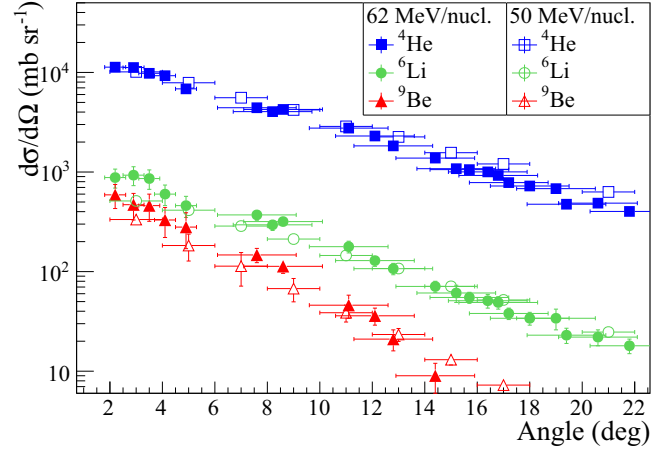
FIG. 12. Comparison with the 62 MeV/nucleon experiment at LNS [4]. The angular distributions of ^{4}He (blue squares), ^{6}Li (green circles), and ^{9}Be (red triangles) are represented. The data of this work are represented by hollow symbols while the data from LNS in full symbols.

VI. CONCLUSION

Fragment production measurements of a 50 MeV/nucleon ^{12}C beam have been performed for 17 different angles and five different targets of medical interest. This led in obtaining the double differential cross sections of ^{12}C on hydrogen, carbon, oxygen, aluminum, and titanium between 3° and 39° for all isotopes from protons to ^{12}C.

The angular distributions are dominated by light fragment emission (protons and α particles) all over the angular range. At forward angles, the α production dominates all other contributions, which could be compatible with an α substructure of the ^{12}C ion. The other fragments cross sections increase with their charge and mass. These behaviors have also been observed with a 95 MeV/nucleon ^{12}C beam during a previous experiment [16].

The energy distributions present a peak close to the beam energy at small angles due to the quasiprojectile emission. The peak energy then decreases for higher angular values. They also present a contribution at low energies for targets other than hydrogen that increases with the charge and mass of the target.

The reconstruction of the cross sections for a PMMA target using only elemental targets has been achieved successfully: it seems possible to compute the fragmentation cross sections for almost any tissue in the human body at 50 and 95 MeV/nucleon [16].

By combining these results with those from the 95 MeV/nucleon ^{12}C beam experiment, the last 2 cm of the ^{12}C range in the body during a treatment are covered. These sets of data (angular and energy distributions for each target) are available for free access on the website http://hadrontherapy-data.in2p3.fr.

To complete these data up to the maximum energy used for treatment (e.g., 400 MeV/nucleon), new measurements are planned in the future ARCHADE research and treatment center in Caen.

ACKNOWLEDGMENTS

APPENDIX A: DIFFERENTIAL CROSS SECTIONS FOR THE HYDROGEN TARGET

TABLE IV. ^{12}C fragmentation cross sections for the hydrogen target at different angles.

θ (deg)	^{1}H $d\sigma/d\Omega$ (b sr^{-1})	^{2}H $d\sigma/d\Omega$ (b sr^{-1})	^{3}H $d\sigma/d\Omega$ (b sr^{-1})	^{3}He $d\sigma/d\Omega$ (b sr^{-1})	^{4}He $d\sigma/d\Omega$ (b sr^{-1})	^{6}He $d\sigma/d\Omega$ (b sr^{-1})
3(1)	$(7.38\pm0.15)\times10^{-1}$	$(2.28\pm0.11)\times10^{-1}$	$(9.99\pm0.66)\times10^{-2}$	$(2.11\pm0.21)\times10^{-1}$	(6.25 ± 0.18)	$(1.14\pm0.62)\times10^{-2}$
5(1)	$(3.69\pm0.53)\times10^{-1}$	$(1.05\pm0.26)\times10^{-1}$	$(7.25\pm0.85)\times10^{-2}$	$(1.33\pm0.49)\times10^{-1}$	(2.94 ± 0.25)	–
7(1)	$(4.34\pm0.57)\times10^{-1}$	$(1.30\pm0.29)\times10^{-1}$	$(4.33\pm0.56)\times10^{-2}$	$(1.28\pm0.47)\times10^{-1}$	(1.66 ± 0.19)	–
9(1)	$(3.84\pm0.16)\times10^{-1}$	$(1.19\pm0.07)\times10^{-1}$	$(3.67\pm1.15)\times10^{-2}$	$(9.44\pm4.11)\times10^{-2}$	$(9.31\pm1.43)\times10^{-1}$	–
11(1)	$(3.82\pm0.15)\times10^{-1}$	$(1.02\pm0.07)\times10^{-1}$	$(3.60\pm0.95)\times10^{-2}$	$(7.19\pm3.56)\times10^{-2}$	$(5.14\pm0.94)\times10^{-1}$	–
13(1)	$(2.80\pm0.11)\times10^{-1}$	$(6.88\pm0.55)\times10^{-2}$	$(1.08\pm0.84)\times10^{-2}$	$(3.87\pm2.51)\times10^{-2}$	$(1.49\pm0.65)\times10^{-1}$	–
15(1)	$(2.46\pm0.11)\times10^{-1}$	$(5.98\pm0.49)\times10^{-2}$	$(7.19\pm6.79)\times10^{-3}$	$(3.04\pm1.92)\times10^{-2}$	$(1.06\pm0.42)\times10^{-1}$	–
17(1)	$(1.81\pm0.07)\times10^{-1}$	$(4.57\pm0.34)\times10^{-2}$	$(2.43\pm4.51)\times10^{-3}$	$(1.41\pm1.06)\times10^{-2}$	$(2.04\pm22.36)\times10^{-3}$	–
21(1)	$(1.17\pm0.06)\times10^{-1}$	$(3.65\pm0.25)\times10^{-2}$	–	$(8.19\pm5.29)\times10^{-3}$	$(4.70\pm876.48)\times10^{-5}$	–
23(1)	$(1.03\pm0.07)\times10^{-1}$	$(4.61\pm0.28)\times10^{-2}$	$(1.45\pm21.17)\times10^{-4}$	$(4.68\pm4.29)\times10^{-3}$	$(1.01\pm5.61)\times10^{-3}$	–
25(1)	$(8.85\pm0.62)\times10^{-2}$	$(3.08\pm0.24)\times10^{-2}$	–	–	–	–
27(1)	$(7.75\pm0.57)\times10^{-2}$	$(2.97\pm0.21)\times10^{-2}$	–	–	–	–
29(1)	$(6.54\pm0.48)\times10^{-2}$	$(3.30\pm0.18)\times10^{-2}$	–	–	–	–
31(1)	$(5.72\pm0.43)\times10^{-2}$	$(4.25\pm0.19)\times10^{-2}$	–	–	–	–
33(1)	$(5.23\pm0.37)\times10^{-2}$	$(2.20\pm0.15)\times10^{-2}$	–	–	–	–
35(1)	$(4.37\pm0.28)\times10^{-2}$	–	–	–	–	–
39(1)	$(3.71\pm0.23)\times10^{-2}$	–	–	–	–	–

θ (deg)	^{6}Li $d\sigma/d\Omega$ (b sr^{-1})	^{7}Li $d\sigma/d\Omega$ (b sr^{-1})	^{7}Be $d\sigma/d\Omega$ (b sr^{-1})	^{9}Be $d\sigma/d\Omega$ (b sr^{-1})	^{10}Be $d\sigma/d\Omega$ (b sr^{-1})	^{8}B $d\sigma/d\Omega$ (b sr^{-1})
3(1)	$(2.65\pm0.05)\times10^{-1}$	$(4.72\pm0.08)\times10^{-1}$	$(6.45\pm0.25)\times10^{-1}$	$(6.00\pm2.74)\times10^{-2}$	$(9.98\pm1.20)\times10^{-2}$	$(7.62\pm124.59)\times10^{-2}$
5(1)	$(1.23\pm0.05)\times10^{-1}$	$(1.61\pm0.07)\times10^{-1}$	$(3.00\pm0.14)\times10^{-1}$	$(2.46\pm4.37)\times10^{-2}$	$(8.35\pm9.38)\times10^{-3}$	$(9.87\pm546.28)\times10^{-3}$
7(1)	$(5.19\pm0.33)\times10^{-2}$	$(4.82\pm0.39)\times10^{-2}$	$(1.07\pm0.09)\times10^{-1}$	$(3.41\pm30.18)\times10^{-3}$	$(3.18\pm5.17)\times10^{-3}$	$(3.53\pm3048.46)\times10^{-4}$
9(1)	$(2.18\pm0.24)\times10^{-2}$	$(1.21\pm0.27)\times10^{-2}$	$(3.31\pm0.24)\times10^{-2}$	–	$(1.01\pm16.62)\times10^{-4}$	–
11(1)	$(6.98\pm1.60)\times10^{-3}$	$(4.26\pm1.67)\times10^{-3}$	$(6.53\pm1.40)\times10^{-3}$	$(1.33\pm5.53)\times10^{-3}$	–	–

θ (deg)	^{10}B $d\sigma/d\Omega$ (b sr^{-1})	^{11}B $d\sigma/d\Omega$ (b sr^{-1})	^{10}C $d\sigma/d\Omega$ (b sr^{-1})	^{11}C $d\sigma/d\Omega$ (b sr^{-1})	^{12}C $d\sigma/d\Omega$ (b sr^{-1})
3(1)	$(6.51\pm0.82)\times10^{-1}$	(1.64 ± 0.02)	$(6.74\pm2.04)\times10^{-1}$	(2.90 ± 1.40)	–
5(1)	$(2.22\pm0.64)\times10^{-1}$	$(2.66\pm0.22)\times10^{-1}$	$(1.11\pm1.47)\times10^{-1}$	(1.38 ± 1.78)	–
7(1)	$(2.31\pm3.44)\times10^{-2}$	–	$(6.09\pm26.38)\times10^{-3}$	$(4.30\pm31.68)\times10^{-2}$	–
9(1)	–	–	–	$(1.33\pm5.07)\times10^{-3}$	–
11(1)	–	–	$(1.34\pm0.29)\times10^{-3}$	$(4.69\pm1.66)\times10^{-3}$	–

APPENDIX B: DIFFERENTIAL CROSS SECTIONS FOR THE CARBON TARGET

TABLE V. ^{12}C fragmentation cross sections for the carbon target at different angles.

θ (deg)	^{1}H $d\sigma/d\Omega$ (b sr^{-1})	^{2}H $d\sigma/d\Omega$ (b sr^{-1})	^{3}H $d\sigma/d\Omega$ (b sr^{-1})	^{3}He $d\sigma/d\Omega$ (b sr^{-1})	^{4}He $d\sigma/d\Omega$ (b sr^{-1})	^{6}He $d\sigma/d\Omega$ (b sr^{-1})
3(1)	(1.58 ± 0.02)	$(8.97\pm0.13)\times10^{-1}$	$(5.50\pm0.08)\times10^{-1}$	$(4.90\pm0.21)\times10^{-1}$	$(1.01\pm0.02)\times10^{1}$	$(4.19\pm0.69)\times10^{-2}$
5(1)	(1.43 ± 0.06)	$(8.78\pm0.32)\times10^{-1}$	$(4.62\pm0.12)\times10^{-1}$	$(4.93\pm0.53)\times10^{-1}$	(7.87 ± 0.25)	$(3.22\pm2.38)\times10^{-2}$
7(1)	(1.27 ± 0.07)	$(7.44\pm0.33)\times10^{-1}$	$(4.41\pm0.08)\times10^{-1}$	$(4.55\pm0.51)\times10^{-1}$	(5.57 ± 0.21)	$(3.17\pm2.58)\times10^{-2}$
9(1)	(1.08 ± 0.02)	$(6.47\pm0.09)\times10^{-1}$	$(3.80\pm0.15)\times10^{-1}$	$(3.62\pm0.45)\times10^{-1}$	(4.20 ± 0.16)	$(1.69\pm1.53)\times10^{-2}$
11(1)	(1.04 ± 0.02)	$(5.93\pm0.08)\times10^{-1}$	$(3.06\pm0.12)\times10^{-1}$	$(3.11\pm0.40)\times10^{-1}$	(2.87 ± 0.11)	$(1.43\pm1.42)\times10^{-2}$
13(1)	$(8.56\pm0.12)\times10^{-1}$	$(5.05\pm0.07)\times10^{-1}$	$(2.79\pm0.11)\times10^{-1}$	$(2.54\pm0.30)\times10^{-1}$	(2.25 ± 0.09)	$(9.58\pm10.02)\times10^{-3}$
15(1)	$(7.90\pm0.11)\times10^{-1}$	$(4.42\pm0.06)\times10^{-1}$	$(2.33\pm0.09)\times10^{-1}$	$(2.06\pm0.23)\times10^{-1}$	(1.56 ± 0.06)	$(8.18\pm8.41)\times10^{-3}$

TABLE V. *(Continued.)*

θ (deg)	^{1}H $d\sigma/d\Omega$ (b sr^{-1})	^{2}H $d\sigma/d\Omega$ (b sr^{-1})	^{3}H $d\sigma/d\Omega$ (b sr^{-1})	^{3}He $d\sigma/d\Omega$ (b sr^{-1})	^{4}He $d\sigma/d\Omega$ (b sr^{-1})	^{6}He $d\sigma/d\Omega$ (b sr^{-1})
17(1)	$(6.56 \pm 0.10) \times 10^{-1}$	$(3.82 \pm 0.05) \times 10^{-1}$	$(1.99 \pm 0.08) \times 10^{-1}$	$(1.71 \pm 0.17) \times 10^{-1}$	(1.21 ± 0.04)	$(4.95 \pm 4.92) \times 10^{-3}$
21(1)	$(5.08 \pm 0.09) \times 10^{-1}$	$(2.79 \pm 0.04) \times 10^{-1}$	$(1.34 \pm 0.04) \times 10^{-1}$	$(1.06 \pm 0.08) \times 10^{-1}$	$(6.31 \pm 0.15) \times 10^{-1}$	$(3.12 \pm 2.56) \times 10^{-3}$
23(1)	$(4.30 \pm 0.08) \times 10^{-1}$	$(2.04 \pm 0.03) \times 10^{-1}$	$(1.04 \pm 0.03) \times 10^{-1}$	$(7.94 \pm 0.56) \times 10^{-2}$	$(4.39 \pm 0.08) \times 10^{-1}$	$(2.01 \pm 1.46) \times 10^{-3}$
25(1)	$(3.41 \pm 0.07) \times 10^{-1}$	$(1.81 \pm 0.03) \times 10^{-1}$	$(8.27 \pm 0.18) \times 10^{-2}$	$(6.05 \pm 0.40) \times 10^{-2}$	$(3.21 \pm 0.05) \times 10^{-1}$	$(1.46 \pm 0.90) \times 10^{-3}$
27(1)	$(3.05 \pm 0.06) \times 10^{-1}$	$(1.60 \pm 0.02) \times 10^{-1}$	$(7.04 \pm 0.13) \times 10^{-2}$	$(4.83 \pm 0.29) \times 10^{-2}$	$(2.57 \pm 0.03) \times 10^{-1}$	$(1.15 \pm 0.64) \times 10^{-3}$
29(1)	$(2.52 \pm 0.05) \times 10^{-1}$	$(1.29 \pm 0.02) \times 10^{-1}$	$(5.44 \pm 0.10) \times 10^{-2}$	$(3.65 \pm 0.20) \times 10^{-2}$	$(1.89 \pm 0.03) \times 10^{-1}$	$(8.36 \pm 4.30) \times 10^{-4}$
31(1)	$(2.39 \pm 0.05) \times 10^{-1}$	$(1.21 \pm 0.02) \times 10^{-1}$	$(4.99 \pm 0.07) \times 10^{-2}$	$(3.15 \pm 0.16) \times 10^{-2}$	$(1.66 \pm 0.03) \times 10^{-1}$	$(7.11 \pm 3.51) \times 10^{-4}$
33(1)	$(2.00 \pm 0.04) \times 10^{-1}$	$(1.00 \pm 0.02) \times 10^{-1}$	$(3.95 \pm 0.05) \times 10^{-2}$	$(2.40 \pm 0.13) \times 10^{-2}$	$(1.28 \pm 0.04) \times 10^{-1}$	$(5.65 \pm 2.82) \times 10^{-4}$
35(1)	$(1.92 \pm 0.04) \times 10^{-1}$	$(9.35 \pm 0.17) \times 10^{-2}$	$(3.63 \pm 0.06) \times 10^{-2}$	$(2.07 \pm 0.13) \times 10^{-2}$	$(1.15 \pm 0.05) \times 10^{-1}$	$(5.09 \pm 2.56) \times 10^{-4}$
39(1)	$(1.46 \pm 0.03) \times 10^{-1}$	$(6.87 \pm 0.15) \times 10^{-2}$	$(2.54 \pm 0.07) \times 10^{-2}$	$(1.30 \pm 0.12) \times 10^{-2}$	$(7.64 \pm 0.65) \times 10^{-2}$	$(3.29 \pm 2.24) \times 10^{-4}$

θ (deg)	^{6}Li $d\sigma/d\Omega$ (b sr^{-1})	^{7}Li $d\sigma/d\Omega$ (b sr^{-1})	^{7}Be $d\sigma/d\Omega$ (b sr^{-1})	^{9}Be $d\sigma/d\Omega$ (b sr^{-1})	^{10}Be $d\sigma/d\Omega$ (b sr^{-1})	^{8}B $d\sigma/d\Omega$ (b sr^{-1})
3(1)	$(5.12 \pm 0.05) \times 10^{-1}$	$(6.05 \pm 0.06) \times 10^{-1}$	$(4.34 \pm 0.17) \times 10^{-1}$	$(3.33 \pm 0.35) \times 10^{-1}$	$(1.65 \pm 0.11) \times 10^{-1}$	$(1.36 \pm 11.15) \times 10^{-1}$
5(1)	$(4.14 \pm 0.06) \times 10^{-1}$	$(4.72 \pm 0.07) \times 10^{-1}$	$(3.48 \pm 0.13) \times 10^{-1}$	$(1.83 \pm 0.55) \times 10^{-1}$	$(1.39 \pm 0.13) \times 10^{-1}$	$(6.35 \pm 66.64) \times 10^{-2}$
7(1)	$(2.87 \pm 0.04) \times 10^{-1}$	$(3.44 \pm 0.05) \times 10^{-1}$	$(2.41 \pm 0.11) \times 10^{-1}$	$(1.13 \pm 0.42) \times 10^{-1}$	$(6.74 \pm 0.72) \times 10^{-2}$	$(3.97 \pm 42.80) \times 10^{-2}$
9(1)	$(2.12 \pm 0.03) \times 10^{-1}$	$(2.37 \pm 0.04) \times 10^{-1}$	$(1.69 \pm 0.03) \times 10^{-1}$	$(6.75 \pm 1.78) \times 10^{-2}$	$(4.05 \pm 0.23) \times 10^{-2}$	$(2.26 \pm 23.05) \times 10^{-2}$
11(1)	$(1.45 \pm 0.02) \times 10^{-1}$	$(1.52 \pm 0.02) \times 10^{-1}$	$(1.09 \pm 0.02) \times 10^{-1}$	$(3.86 \pm 0.75) \times 10^{-2}$	$(2.27 \pm 0.11) \times 10^{-2}$	$(9.48 \pm 75.47) \times 10^{-3}$
13(1)	$(1.07 \pm 0.02) \times 10^{-1}$	$(1.12 \pm 0.02) \times 10^{-1}$	$(7.78 \pm 0.13) \times 10^{-2}$	$(2.34 \pm 0.35) \times 10^{-2}$	$(1.35 \pm 0.05) \times 10^{-2}$	$(7.53 \pm 42.13) \times 10^{-3}$
15(1)	$(7.11 \pm 0.15) \times 10^{-2}$	$(7.23 \pm 0.10) \times 10^{-2}$	$(4.85 \pm 0.08) \times 10^{-2}$	$(1.30 \pm 0.15) \times 10^{-2}$	$(6.15 \pm 0.23) \times 10^{-3}$	$(3.24 \pm 14.97) \times 10^{-3}$
17(1)	$(5.19 \pm 0.09) \times 10^{-2}$	$(4.85 \pm 0.07) \times 10^{-2}$	$(3.26 \pm 0.05) \times 10^{-2}$	$(7.25 \pm 0.67) \times 10^{-3}$	$(3.66 \pm 0.12) \times 10^{-3}$	$(3.00 \pm 10.96) \times 10^{-3}$
21(1)	$(2.47 \pm 0.04) \times 10^{-2}$	$(2.11 \pm 0.04) \times 10^{-2}$	$(1.33 \pm 0.02) \times 10^{-2}$	$(2.41 \pm 0.17) \times 10^{-3}$	$(8.56 \pm 0.43) \times 10^{-4}$	$(7.44 \pm 18.55) \times 10^{-4}$
23(1)	$(1.62 \pm 0.03) \times 10^{-2}$	$(1.28 \pm 0.04) \times 10^{-2}$	$(7.95 \pm 0.24) \times 10^{-3}$	$(1.34 \pm 0.11) \times 10^{-3}$	$(4.36 \pm 0.50) \times 10^{-4}$	$(6.81 \pm 15.16) \times 10^{-4}$
25(1)	$(1.09 \pm 0.02) \times 10^{-2}$	$(8.72 \pm 0.33) \times 10^{-3}$	$(4.96 \pm 0.21) \times 10^{-3}$	$(8.13 \pm 0.86) \times 10^{-4}$	$(2.38 \pm 0.36) \times 10^{-4}$	$(2.91 \pm 4.72) \times 10^{-4}$
27(1)	$(8.62 \pm 0.26) \times 10^{-3}$	$(6.03 \pm 0.33) \times 10^{-3}$	$(3.33 \pm 0.17) \times 10^{-3}$	$(5.47 \pm 0.64) \times 10^{-4}$	$(1.66 \pm 0.39) \times 10^{-4}$	$(2.44 \pm 3.35) \times 10^{-4}$
29(1)	$(5.63 \pm 0.19) \times 10^{-3}$	$(4.64 \pm 0.27) \times 10^{-3}$	$(2.18 \pm 0.12) \times 10^{-3}$	$(3.35 \pm 0.51) \times 10^{-4}$	$(1.04 \pm 0.35) \times 10^{-4}$	$(1.38 \pm 1.42) \times 10^{-4}$
31(1)	$(5.09 \pm 0.22) \times 10^{-3}$	$(3.46 \pm 0.38) \times 10^{-3}$	$(1.76 \pm 0.20) \times 10^{-3}$	$(2.51 \pm 0.96) \times 10^{-4}$	$(6.48 \pm 5.16) \times 10^{-5}$	$(1.44 \pm 3.60) \times 10^{-4}$
33(1)	$(3.43 \pm 0.32) \times 10^{-3}$	$(2.65 \pm 0.51) \times 10^{-3}$	$(1.21 \pm 0.19) \times 10^{-3}$	$(1.82 \pm 1.49) \times 10^{-4}$	$(7.30 \pm 11.71) \times 10^{-5}$	$(6.16 \pm 19.19) \times 10^{-5}$
35(1)	$(3.23 \pm 0.40) \times 10^{-3}$	$(2.16 \pm 0.76) \times 10^{-3}$	$(9.36 \pm 3.32) \times 10^{-4}$	$(1.81 \pm 5.53) \times 10^{-4}$	$(4.57 \pm 47.68) \times 10^{-5}$	$(6.68 \pm 5.62) \times 10^{-5}$
39(1)	$(1.72 \pm 0.78) \times 10^{-3}$	$(1.37 \pm 1.02) \times 10^{-3}$	$(5.13 \pm 15.55) \times 10^{-4}$	$(9.74 \pm 59.19) \times 10^{-5}$	$(2.89 \pm 69.88) \times 10^{-5}$	$(2.34 \pm 0.36) \times 10^{-5}$

θ (deg)	^{10}B $d\sigma/d\Omega$ (b sr^{-1})	^{11}B $d\sigma/d\Omega$ (b sr^{-1})	^{10}C $d\sigma/d\Omega$ (b sr^{-1})	^{11}C $d\sigma/d\Omega$ (b sr^{-1})	^{12}C $d\sigma/d\Omega$ (b sr^{-1})
3(1)	(1.09 ± 0.08)	(1.41 ± 0.02)	$(7.45 \pm 1.33) \times 10^{-1}$	(2.05 ± 0.76)	$(8.97 \pm 0.13) \times 10^{-3}$
5(1)	$(5.38 \pm 0.73) \times 10^{-1}$	$(8.47 \pm 0.33) \times 10^{-1}$	$(2.99 \pm 1.21) \times 10^{-1}$	(2.62 ± 1.82)	$(1.04 \pm 0.02) \times 10^{-1}$
7(1)	$(3.20 \pm 0.48) \times 10^{-1}$	$(3.66 \pm 0.21) \times 10^{-1}$	$(8.86 \pm 3.66) \times 10^{-2}$	$(7.80 \pm 4.48) \times 10^{-1}$	$(3.32 \pm 0.10) \times 10^{-3}$
9(1)	$(1.88 \pm 0.18) \times 10^{-1}$	$(1.93 \pm 0.03) \times 10^{-1}$	$(5.66 \pm 0.10) \times 10^{-2}$	$(3.83 \pm 0.07) \times 10^{-1}$	$(5.89 \pm 0.18) \times 10^{-3}$
11(1)	$(9.66 \pm 0.99) \times 10^{-2}$	$(8.43 \pm 0.11) \times 10^{-2}$	$(1.96 \pm 0.03) \times 10^{-2}$	$(1.22 \pm 0.02) \times 10^{-1}$	$(1.85 \pm 0.10) \times 10^{-3}$
13(1)	$(5.48 \pm 0.72) \times 10^{-2}$	$(4.61 \pm 0.06) \times 10^{-2}$	$(1.18 \pm 0.02) \times 10^{-2}$	$(5.91 \pm 0.15) \times 10^{-2}$	$(1.04 \pm 0.06) \times 10^{-3}$
15(1)	$(2.74 \pm 0.46) \times 10^{-2}$	$(1.71 \pm 0.03) \times 10^{-2}$	$(4.75 \pm 0.10) \times 10^{-3}$	$(1.79 \pm 0.05) \times 10^{-2}$	$(6.68 \pm 0.50) \times 10^{-4}$
17(1)	$(1.37 \pm 0.28) \times 10^{-2}$	$(8.42 \pm 0.15) \times 10^{-3}$	$(2.55 \pm 0.06) \times 10^{-3}$	$(7.16 \pm 0.25) \times 10^{-3}$	$(4.30 \pm 0.42) \times 10^{-4}$
21(1)	$(3.59 \pm 1.22) \times 10^{-3}$	$(1.49 \pm 0.06) \times 10^{-3}$	$(5.16 \pm 0.19) \times 10^{-4}$	$(9.29 \pm 0.24) \times 10^{-4}$	$(1.61 \pm 0.26) \times 10^{-4}$
23(1)	$(1.63 \pm 0.75) \times 10^{-3}$	$(6.87 \pm 0.69) \times 10^{-4}$	$(2.08 \pm 0.13) \times 10^{-4}$	$(3.32 \pm 0.21) \times 10^{-4}$	$(8.72 \pm 2.57) \times 10^{-5}$
25(1)	$(8.28 \pm 5.03) \times 10^{-4}$	$(4.28 \pm 0.79) \times 10^{-4}$	$(1.22 \pm 0.19) \times 10^{-4}$	$(1.66 \pm 0.20) \times 10^{-4}$	$(5.31 \pm 2.31) \times 10^{-5}$
27(1)	$(5.84 \pm 5.06) \times 10^{-4}$	$(1.53 \pm 0.60) \times 10^{-4}$	$(5.63 \pm 1.16) \times 10^{-5}$	$(6.25 \pm 2.39) \times 10^{-5}$	$(3.13 \pm 1.42) \times 10^{-5}$
29(1)	$(3.24 \pm 3.69) \times 10^{-4}$	$(1.55 \pm 1.81) \times 10^{-4}$	$(3.38 \pm 0.73) \times 10^{-5}$	$(5.35 \pm 7.73) \times 10^{-5}$	$(1.97 \pm 1.07) \times 10^{-5}$
31(1)	$(2.53 \pm 6.26) \times 10^{-4}$	$(9.08 \pm 61.68) \times 10^{-5}$	$(2.35 \pm 9.84) \times 10^{-5}$	$(2.76 \pm 35.38) \times 10^{-5}$	$(8.92 \pm 5.32) \times 10^{-6}$
33(1)	$(1.72 \pm 15.27) \times 10^{-4}$	$(5.84 \pm 148.54) \times 10^{-5}$	$(1.30 \pm 2.92) \times 10^{-5}$	$(1.62 \pm 78.18) \times 10^{-5}$	$(8.11 \pm 4.54) \times 10^{-6}$
35(1)	$(1.15 \pm 87.66) \times 10^{-4}$	$(3.73 \pm 0.46) \times 10^{-5}$	$(1.78 \pm 0.32) \times 10^{-5}$	$(1.17 \pm 0.26) \times 10^{-5}$	$(3.34 \pm 2.96) \times 10^{-6}$
39(1)	$(5.07 \pm 0.54) \times 10^{-5}$	$(2.89 \pm 0.40) \times 10^{-5}$	$(3.34 \pm 1.36) \times 10^{-6}$	$(6.68 \pm 1.93) \times 10^{-6}$	$(1.67 \pm 2.97) \times 10^{-6}$

APPENDIX C: DIFFERENTIAL CROSS SECTIONS FOR THE OXYGEN TARGET

TABLE VI. ^{12}C fragmentation cross sections for the oxygen target at different angles.

θ (deg)	^{1}H $d\sigma/d\Omega$ (b sr^{-1})	^{2}H $d\sigma/d\Omega$ (b sr^{-1})	^{3}H $d\sigma/d\Omega$ (b sr^{-1})	^{3}He $d\sigma/d\Omega$ (b sr^{-1})	^{4}He $d\sigma/d\Omega$ (b sr^{-1})	^{6}He $d\sigma/d\Omega$ (b sr^{-1})
3(1)	(1.92 ± 0.04)	(1.08 ± 0.03)	$(6.25 \pm 0.17) \times 10^{-1}$	$(6.13 \pm 0.51) \times 10^{-1}$	$(1.17 \pm 0.04) \times 10^{1}$	$(5.14 \pm 1.78) \times 10^{-2}$
5(1)	(1.45 ± 0.15)	$(9.06 \pm 0.72) \times 10^{-1}$	$(5.41 \pm 0.18) \times 10^{-1}$	$(5.67 \pm 1.16) \times 10^{-1}$	(7.99 ± 0.47)	$(4.36 \pm 5.96) \times 10^{-2}$
7(1)	(1.44 ± 0.16)	$(8.47 \pm 0.73) \times 10^{-1}$	$(4.97 \pm 0.15) \times 10^{-1}$	$(4.92 \pm 1.10) \times 10^{-1}$	(5.97 ± 0.40)	$(3.46 \pm 5.36) \times 10^{-2}$
9(1)	(1.25 ± 0.04)	$(7.56 \pm 0.20) \times 10^{-1}$	$(4.34 \pm 0.34) \times 10^{-1}$	$(4.23 \pm 1.01) \times 10^{-1}$	(4.50 ± 0.32)	$(2.28 \pm 3.80) \times 10^{-2}$
11(1)	(1.23 ± 0.03)	$(7.09 \pm 0.18) \times 10^{-1}$	$(3.80 \pm 0.30) \times 10^{-1}$	$(3.59 \pm 0.91) \times 10^{-1}$	(3.40 ± 0.24)	$(1.86 \pm 3.54) \times 10^{-2}$
13(1)	$(9.90 \pm 0.26) \times 10^{-1}$	$(5.92 \pm 0.15) \times 10^{-1}$	$(3.23 \pm 0.27) \times 10^{-1}$	$(2.95 \pm 0.69) \times 10^{-1}$	(2.45 ± 0.17)	$(1.19 \pm 2.54) \times 10^{-2}$
15(1)	$(9.34 \pm 0.26) \times 10^{-1}$	$(5.32 \pm 0.14) \times 10^{-1}$	$(2.75 \pm 0.23) \times 10^{-1}$	$(2.40 \pm 0.54) \times 10^{-1}$	(1.81 ± 0.12)	$(1.02 \pm 2.14) \times 10^{-2}$
17(1)	$(7.29 \pm 0.22) \times 10^{-1}$	$(4.29 \pm 0.12) \times 10^{-1}$	$(2.20 \pm 0.19) \times 10^{-1}$	$(1.94 \pm 0.40) \times 10^{-1}$	(1.32 ± 0.09)	$(6.66 \pm 14.58) \times 10^{-3}$
21(1)	$(5.93 \pm 0.20) \times 10^{-1}$	$(3.33 \pm 0.10) \times 10^{-1}$	$(1.53 \pm 0.11) \times 10^{-1}$	$(1.28 \pm 0.21) \times 10^{-1}$	$(7.58 \pm 0.39) \times 10^{-1}$	$(3.94 \pm 7.82) \times 10^{-3}$
23(1)	$(5.08 \pm 0.19) \times 10^{-1}$	$(2.79 \pm 0.08) \times 10^{-1}$	$(1.26 \pm 0.08) \times 10^{-1}$	$(1.03 \pm 0.14) \times 10^{-1}$	$(5.53 \pm 0.22) \times 10^{-1}$	$(2.59 \pm 4.44) \times 10^{-3}$
25(1)	$(4.35 \pm 0.17) \times 10^{-1}$	$(2.34 \pm 0.07) \times 10^{-1}$	$(1.04 \pm 0.05) \times 10^{-1}$	$(8.03 \pm 1.03) \times 10^{-2}$	$(4.25 \pm 0.14) \times 10^{-1}$	$(2.04 \pm 2.93) \times 10^{-3}$
27(1)	$(3.84 \pm 0.16) \times 10^{-1}$	$(2.06 \pm 0.06) \times 10^{-1}$	$(8.71 \pm 0.38) \times 10^{-2}$	$(6.53 \pm 0.75) \times 10^{-2}$	$(3.35 \pm 0.09) \times 10^{-1}$	$(1.54 \pm 1.97) \times 10^{-3}$
29(1)	$(3.28 \pm 0.13) \times 10^{-1}$	$(1.68 \pm 0.05) \times 10^{-1}$	$(6.99 \pm 0.30) \times 10^{-2}$	$(5.10 \pm 0.54) \times 10^{-2}$	$(2.53 \pm 0.07) \times 10^{-1}$	$(8.85 \pm 13.03) \times 10^{-4}$
31(1)	$(2.96 \pm 0.12) \times 10^{-1}$	$(1.51 \pm 0.05) \times 10^{-1}$	$(5.87 \pm 0.19) \times 10^{-2}$	$(4.08 \pm 0.46) \times 10^{-2}$	$(2.01 \pm 0.10) \times 10^{-1}$	$(8.33 \pm 11.63) \times 10^{-4}$
33(1)	$(2.56 \pm 0.11) \times 10^{-1}$	$(1.26 \pm 0.04) \times 10^{-1}$	$(4.85 \pm 0.15) \times 10^{-2}$	$(3.16 \pm 0.38) \times 10^{-2}$	$(1.57 \pm 0.11) \times 10^{-1}$	$(5.94 \pm 8.75) \times 10^{-4}$
35(1)	$(2.31 \pm 0.11) \times 10^{-1}$	$(1.13 \pm 0.05) \times 10^{-1}$	$(4.04 \pm 0.15) \times 10^{-2}$	$(2.57 \pm 0.37) \times 10^{-2}$	$(1.30 \pm 0.15) \times 10^{-1}$	$(5.10 \pm 7.94) \times 10^{-4}$
39(1)	$(1.82 \pm 0.09) \times 10^{-1}$	$(8.39 \pm 0.41) \times 10^{-2}$	$(2.81 \pm 0.18) \times 10^{-2}$	$(1.65 \pm 0.35) \times 10^{-2}$	$(8.51 \pm 1.86) \times 10^{-2}$	$(3.60 \pm 6.81) \times 10^{-4}$

θ (deg)	^{6}Li $d\sigma/d\Omega$ (b sr^{-1})	^{7}Li $d\sigma/d\Omega$ (b sr^{-1})	^{7}Be $d\sigma/d\Omega$ (b sr^{-1})	^{9}Be $d\sigma/d\Omega$ (b sr^{-1})	^{10}Be $d\sigma/d\Omega$ (b sr^{-1})	^{8}B $d\sigma/d\Omega$ (b sr^{-1})
3(1)	$(5.87 \pm 0.10) \times 10^{-1}$	$(6.34 \pm 0.13) \times 10^{-1}$	$(5.12 \pm 0.33) \times 10^{-1}$	$(3.87 \pm 0.79) \times 10^{-1}$	$(1.86 \pm 0.23) \times 10^{-1}$	$(1.41 \pm 23.33) \times 10^{-1}$
5(1)	$(4.14 \pm 0.10) \times 10^{-1}$	$(4.93 \pm 0.13) \times 10^{-1}$	$(3.50 \pm 0.21) \times 10^{-1}$	$(1.79 \pm 0.98) \times 10^{-1}$	$(1.31 \pm 0.20) \times 10^{-1}$	$(5.37 \pm 98.21) \times 10^{-2}$
7(1)	$(3.15 \pm 0.08) \times 10^{-1}$	$(3.59 \pm 0.09) \times 10^{-1}$	$(2.60 \pm 0.18) \times 10^{-1}$	$(1.21 \pm 0.79) \times 10^{-1}$	$(6.92 \pm 1.23) \times 10^{-2}$	$(3.71 \pm 67.18) \times 10^{-2}$
9(1)	$(2.29 \pm 0.06) \times 10^{-1}$	$(2.54 \pm 0.07) \times 10^{-1}$	$(1.84 \pm 0.05) \times 10^{-1}$	$(7.09 \pm 3.28) \times 10^{-2}$	$(4.47 \pm 0.45) \times 10^{-2}$	$(2.18 \pm 37.15) \times 10^{-2}$
11(1)	$(1.76 \pm 0.05) \times 10^{-1}$	$(1.80 \pm 0.05) \times 10^{-1}$	$(1.31 \pm 0.04) \times 10^{-1}$	$(4.91 \pm 1.65) \times 10^{-2}$	$(2.58 \pm 0.22) \times 10^{-2}$	$(1.29 \pm 16.67) \times 10^{-2}$
13(1)	$(1.20 \pm 0.04) \times 10^{-1}$	$(1.24 \pm 0.04) \times 10^{-1}$	$(8.67 \pm 0.27) \times 10^{-2}$	$(2.79 \pm 0.77) \times 10^{-2}$	$(1.50 \pm 0.12) \times 10^{-2}$	$(8.57 \pm 92.81) \times 10^{-3}$
15(1)	$(9.02 \pm 0.33) \times 10^{-2}$	$(8.36 \pm 0.24) \times 10^{-2}$	$(6.14 \pm 0.19) \times 10^{-2}$	$(1.80 \pm 0.41) \times 10^{-2}$	$(8.62 \pm 0.66) \times 10^{-3}$	$(4.41 \pm 39.55) \times 10^{-3}$
17(1)	$(5.99 \pm 0.22) \times 10^{-2}$	$(5.48 \pm 0.18) \times 10^{-2}$	$(3.81 \pm 0.13) \times 10^{-2}$	$(9.08 \pm 1.89) \times 10^{-3}$	$(4.79 \pm 0.36) \times 10^{-3}$	$(3.29 \pm 29.58) \times 10^{-3}$
21(1)	$(3.35 \pm 0.10) \times 10^{-2}$	$(2.58 \pm 0.12) \times 10^{-2}$	$(1.78 \pm 0.07) \times 10^{-2}$	$(3.65 \pm 0.67) \times 10^{-3}$	$(1.49 \pm 0.18) \times 10^{-3}$	$(9.47 \pm 64.44) \times 10^{-4}$
23(1)	$(2.23 \pm 0.07) \times 10^{-2}$	$(1.67 \pm 0.10) \times 10^{-2}$	$(1.11 \pm 0.06) \times 10^{-2}$	$(2.42 \pm 0.36) \times 10^{-3}$	$(6.72 \pm 1.38) \times 10^{-4}$	$(1.06 \pm 5.63) \times 10^{-3}$
25(1)	$(1.56 \pm 0.05) \times 10^{-2}$	$(1.11 \pm 0.09) \times 10^{-2}$	$(7.64 \pm 0.52) \times 10^{-3}$	$(1.19 \pm 0.27) \times 10^{-3}$	$(3.55 \pm 1.08) \times 10^{-4}$	$(5.69 \pm 20.93) \times 10^{-4}$
27(1)	$(1.18 \pm 0.06) \times 10^{-2}$	$(8.49 \pm 0.90) \times 10^{-3}$	$(4.67 \pm 0.43) \times 10^{-3}$	$(8.11 \pm 1.94) \times 10^{-4}$	$(1.35 \pm 1.17) \times 10^{-4}$	$(4.51 \pm 15.31) \times 10^{-4}$
29(1)	$(7.84 \pm 0.46) \times 10^{-3}$	$(5.37 \pm 0.71) \times 10^{-3}$	$(3.28 \pm 0.33) \times 10^{-3}$	$(6.13 \pm 1.75) \times 10^{-4}$	$(1.61 \pm 1.46) \times 10^{-4}$	$(1.55 \pm 5.05) \times 10^{-4}$
31(1)	$(6.23 \pm 0.66) \times 10^{-3}$	$(3.97 \pm 1.18) \times 10^{-3}$	$(1.97 \pm 0.60) \times 10^{-3}$	$(3.43 \pm 4.25) \times 10^{-4}$	$(6.75 \pm 24.23) \times 10^{-5}$	$(2.24 \pm 14.80) \times 10^{-4}$
33(1)	$(4.22 \pm 1.00) \times 10^{-3}$	$(2.85 \pm 1.64) \times 10^{-3}$	$(1.35 \pm 0.60) \times 10^{-3}$	$(2.60 \pm 6.66) \times 10^{-4}$	$(9.71 \pm 51.53) \times 10^{-5}$	$(1.23 \pm 8.93) \times 10^{-4}$
35(1)	$(3.54 \pm 1.18) \times 10^{-3}$	$(2.22 \pm 2.29) \times 10^{-3}$	$(9.91 \pm 10.71) \times 10^{-4}$	$(1.89 \pm 19.56) \times 10^{-4}$	$(3.13 \pm 163.02) \times 10^{-5}$	$(6.20 \pm 21.76) \times 10^{-5}$
39(1)	$(1.89 \pm 2.42) \times 10^{-3}$	$(1.29 \pm 2.96) \times 10^{-3}$	$(5.56 \pm 48.48) \times 10^{-4}$	$(1.28 \pm 21.34) \times 10^{-4}$	$(6.33 \pm 336.23) \times 10^{-5}$	$(3.04 \pm 1.13) \times 10^{-5}$

θ (deg)	^{10}B $d\sigma/d\Omega$ (b sr^{-1})	^{11}B $d\sigma/d\Omega$ (b sr^{-1})	^{10}C $d\sigma/d\Omega$ (b sr^{-1})	^{11}C $d\sigma/d\Omega$ (b sr^{-1})	^{12}C $d\sigma/d\Omega$ (b sr^{-1})
3(1)	(1.25 ± 0.17)	(1.61 ± 0.03)	$(9.28 \pm 2.96) \times 10^{-1}$	(3.21 ± 1.88)	$(1.75 \pm 0.03) \times 10^{-2}$
5(1)	$(5.22 \pm 1.07) \times 10^{-1}$	$(7.67 \pm 0.37) \times 10^{-1}$	$(2.02 \pm 1.64) \times 10^{-1}$	(2.13 ± 2.77)	$(4.17 \pm 0.16) \times 10^{-3}$
7(1)	$(3.36 \pm 0.78) \times 10^{-1}$	$(3.53 \pm 0.28) \times 10^{-1}$	$(8.99 \pm 6.01) \times 10^{-2}$	$(8.07 \pm 7.84) \times 10^{-1}$	$(4.36 \pm 0.18) \times 10^{-3}$
9(1)	$(1.88 \pm 0.29) \times 10^{-1}$	$(1.90 \pm 0.05) \times 10^{-1}$	$(5.47 \pm 0.15) \times 10^{-2}$	$(3.53 \pm 0.11) \times 10^{-1}$	$(3.52 \pm 0.24) \times 10^{-3}$
11(1)	$(1.25 \pm 0.21) \times 10^{-1}$	$(9.54 \pm 0.23) \times 10^{-2}$	$(2.65 \pm 0.07) \times 10^{-2}$	$(1.60 \pm 0.05) \times 10^{-1}$	$(2.45 \pm 0.22) \times 10^{-3}$
13(1)	$(6.50 \pm 1.50) \times 10^{-2}$	$(4.84 \pm 0.12) \times 10^{-2}$	$(1.62 \pm 0.04) \times 10^{-2}$	$(6.97 \pm 0.31) \times 10^{-2}$	$(1.43 \pm 0.19) \times 10^{-3}$
15(1)	$(3.84 \pm 1.21) \times 10^{-2}$	$(2.26 \pm 0.07) \times 10^{-2}$	$(7.49 \pm 0.29) \times 10^{-3}$	$(2.82 \pm 0.15) \times 10^{-2}$	$(1.20 \pm 0.21) \times 10^{-3}$
17(1)	$(1.75 \pm 0.80) \times 10^{-2}$	$(1.09 \pm 0.04) \times 10^{-2}$	$(3.59 \pm 0.19) \times 10^{-3}$	$(1.01 \pm 0.08) \times 10^{-2}$	$(6.10 \pm 1.62) \times 10^{-4}$
21(1)	$(6.05 \pm 5.22) \times 10^{-3}$	$(2.30 \pm 0.28) \times 10^{-3}$	$(9.52 \pm 1.09) \times 10^{-4}$	$(1.93 \pm 0.19) \times 10^{-3}$	$(2.95 \pm 1.66) \times 10^{-4}$
23(1)	$(2.65 \pm 3.22) \times 10^{-3}$	$(9.79 \pm 2.40) \times 10^{-4}$	$(5.38 \pm 0.19) \times 10^{-4}$	$(8.91 \pm 0.36) \times 10^{-4}$	$(1.41 \pm 1.07) \times 10^{-4}$
25(1)	$(1.31 \pm 2.40) \times 10^{-3}$	$(6.60 \pm 3.09) \times 10^{-4}$	$(2.80 \pm 0.45) \times 10^{-4}$	$(3.80 \pm 0.42) \times 10^{-4}$	$(1.34 \pm 1.33) \times 10^{-4}$
27(1)	$(7.58 \pm 22.17) \times 10^{-4}$	$(3.48 \pm 3.83) \times 10^{-4}$	$(1.12 \pm 0.25) \times 10^{-4}$	$(1.44 \pm 1.58) \times 10^{-4}$	$(3.21 \pm 5.10) \times 10^{-5}$
29(1)	$(6.10 \pm 19.67) \times 10^{-4}$	$(2.07 \pm 9.29) \times 10^{-4}$	$(7.58 \pm 1.16) \times 10^{-5}$	$(1.20 \pm 4.81) \times 10^{-4}$	$(4.12 \pm 5.80) \times 10^{-5}$
31(1)	$(3.85 \pm 30.45) \times 10^{-4}$	$(7.49 \pm 306.28) \times 10^{-5}$	$(6.22 \pm 70.71) \times 10^{-5}$	$(2.26 \pm 264.16) \times 10^{-5}$	$(3.75 \pm 4.97) \times 10^{-5}$
33(1)	$(2.44 \pm 70.64) \times 10^{-4}$	$(5.86 \pm 967.93) \times 10^{-5}$	$(3.01 \pm 23.31) \times 10^{-5}$	$(5.63 \pm 6257.64) \times 10^{-6}$	$(1.21 \pm 2.90) \times 10^{-5}$
35(1)	$(1.27 \pm 402.56) \times 10^{-4}$	$(3.44 \pm 1.67) \times 10^{-5}$	$(1.14 \pm 1.01) \times 10^{-5}$	–	$(1.65 \pm 2.91) \times 10^{-5}$
39(1)	$(5.55 \pm 1.94) \times 10^{-5}$	$(1.58 \pm 1.19) \times 10^{-5}$	$(5.81 \pm 6.16) \times 10^{-6}$	$(8.60 \pm 70.61) \times 10^{-7}$	–

APPENDIX D: DIFFERENTIAL CROSS SECTIONS FOR THE ALUMINUM TARGET

TABLE VII. ^{12}C fragmentation cross sections for the aluminum target at different angles.

θ (deg)	^{1}H $d\sigma/d\Omega$ (b sr^{-1})	^{2}H $d\sigma/d\Omega$ (b sr^{-1})	^{3}H $d\sigma/d\Omega$ (b sr^{-1})	^{3}He $d\sigma/d\Omega$ (b sr^{-1})	^{4}He $d\sigma/d\Omega$ (b sr^{-1})	^{6}He $d\sigma/d\Omega$ (b sr^{-1})
3(1)	(2.39 ± 0.03)	(1.35 ± 0.02)	$(8.40 \pm 0.11) \times 10^{-1}$	$(7.74 \pm 0.32) \times 10^{-1}$	$(1.37 \pm 0.02) \times 10^1$	$(6.97 \pm 1.15) \times 10^{-2}$
5(1)	(1.62 ± 0.10)	(1.03 ± 0.04)	$(6.47 \pm 0.11) \times 10^{-1}$	$(6.49 \pm 0.69) \times 10^{-1}$	(8.32 ± 0.27)	$(4.68 \pm 3.44) \times 10^{-2}$
7(1)	(1.63 ± 0.10)	$(9.82 \pm 0.44) \times 10^{-1}$	$(6.06 \pm 0.09) \times 10^{-1}$	$(6.03 \pm 0.67) \times 10^{-1}$	(6.14 ± 0.23)	$(3.91 \pm 3.18) \times 10^{-2}$
9(1)	(1.39 ± 0.02)	$(8.67 \pm 0.12) \times 10^{-1}$	$(5.27 \pm 0.21) \times 10^{-1}$	$(4.86 \pm 0.60) \times 10^{-1}$	(4.56 ± 0.18)	$(2.43 \pm 2.19) \times 10^{-2}$
11(1)	(1.35 ± 0.02)	$(8.03 \pm 0.11) \times 10^{-1}$	$(4.64 \pm 0.19) \times 10^{-1}$	$(4.32 \pm 0.55) \times 10^{-1}$	(3.36 ± 0.13)	$(2.15 \pm 2.12) \times 10^{-2}$
13(1)	(1.12 ± 0.02)	$(6.87 \pm 0.09) \times 10^{-1}$	$(4.01 \pm 0.16) \times 10^{-1}$	$(3.45 \pm 0.41) \times 10^{-1}$	(2.62 ± 0.10)	$(1.52 \pm 1.59) \times 10^{-2}$
15(1)	(1.06 ± 0.02)	$(6.13 \pm 0.08) \times 10^{-1}$	$(3.51 \pm 0.14) \times 10^{-1}$	$(2.94 \pm 0.33) \times 10^{-1}$	(2.01 ± 0.07)	$(1.31 \pm 1.34) \times 10^{-2}$
17(1)	$(9.34 \pm 0.14) \times 10^{-1}$	$(5.71 \pm 0.08) \times 10^{-1}$	$(3.15 \pm 0.12) \times 10^{-1}$	$(2.54 \pm 0.25) \times 10^{-1}$	(1.68 ± 0.05)	$(9.75 \pm 9.68) \times 10^{-3}$
21(1)	$(7.53 \pm 0.13) \times 10^{-1}$	$(4.34 \pm 0.06) \times 10^{-1}$	$(2.31 \pm 0.08) \times 10^{-1}$	$(1.73 \pm 0.14) \times 10^{-1}$	(1.03 ± 0.02)	$(6.73 \pm 5.51) \times 10^{-3}$
23(1)	$(6.21 \pm 0.11) \times 10^{-1}$	$(3.48 \pm 0.05) \times 10^{-1}$	$(1.73 \pm 0.05) \times 10^{-1}$	$(1.27 \pm 0.09) \times 10^{-1}$	$(7.16 \pm 0.14) \times 10^{-1}$	$(4.34 \pm 3.10) \times 10^{-3}$
25(1)	$(5.26 \pm 0.10) \times 10^{-1}$	$(2.94 \pm 0.05) \times 10^{-1}$	$(1.43 \pm 0.03) \times 10^{-1}$	$(1.01 \pm 0.06) \times 10^{-1}$	$(5.54 \pm 0.09) \times 10^{-1}$	$(3.47 \pm 2.06) \times 10^{-3}$
27(1)	$(4.79 \pm 0.10) \times 10^{-1}$	$(2.60 \pm 0.04) \times 10^{-1}$	$(1.22 \pm 0.02) \times 10^{-1}$	$(8.29 \pm 0.47) \times 10^{-2}$	$(4.54 \pm 0.06) \times 10^{-1}$	$(2.59 \pm 1.38) \times 10^{-3}$
29(1)	$(4.05 \pm 0.08) \times 10^{-1}$	$(2.23 \pm 0.03) \times 10^{-1}$	$(1.00 \pm 0.02) \times 10^{-1}$	$(6.63 \pm 0.34) \times 10^{-2}$	$(3.63 \pm 0.05) \times 10^{-1}$	$(2.07 \pm 1.01) \times 10^{-3}$
31(1)	$(3.89 \pm 0.08) \times 10^{-1}$	$(2.04 \pm 0.03) \times 10^{-1}$	$(8.90 \pm 0.13) \times 10^{-2}$	$(5.69 \pm 0.30) \times 10^{-2}$	$(3.12 \pm 0.07) \times 10^{-1}$	$(1.81 \pm 0.88) \times 10^{-3}$
33(1)	$(3.38 \pm 0.07) \times 10^{-1}$	$(1.73 \pm 0.03) \times 10^{-1}$	$(7.42 \pm 0.10) \times 10^{-2}$	$(4.56 \pm 0.25) \times 10^{-2}$	$(2.54 \pm 0.07) \times 10^{-1}$	$(1.37 \pm 0.67) \times 10^{-3}$
35(1)	$(3.42 \pm 0.07) \times 10^{-1}$	$(1.70 \pm 0.03) \times 10^{-1}$	$(7.00 \pm 0.11) \times 10^{-2}$	$(4.11 \pm 0.26) \times 10^{-2}$	$(2.33 \pm 0.10) \times 10^{-1}$	$(1.25 \pm 0.63) \times 10^{-3}$
39(1)	$(2.68 \pm 0.06) \times 10^{-1}$	$(1.26 \pm 0.03) \times 10^{-1}$	$(4.93 \pm 0.13) \times 10^{-2}$	$(2.67 \pm 0.24) \times 10^{-2}$	$(1.59 \pm 0.14) \times 10^{-1}$	$(7.61 \pm 5.15) \times 10^{-4}$

θ (deg)	^{6}Li $d\sigma/d\Omega$ (b sr^{-1})	^{7}Li $d\sigma/d\Omega$ (b sr^{-1})	^{7}Be $d\sigma/d\Omega$ (b sr^{-1})	^{9}Be $d\sigma/d\Omega$ (b sr^{-1})	^{10}Be $d\sigma/d\Omega$ (b sr^{-1})	^{8}B $d\sigma/d\Omega$ (b sr^{-1})
3(1)	$(6.82 \pm 0.06) \times 10^{-1}$	$(7.95 \pm 0.08) \times 10^{-1}$	$(5.84 \pm 0.19) \times 10^{-1}$	$(5.04 \pm 0.50) \times 10^{-1}$	$(2.40 \pm 0.14) \times 10^{-1}$	$(1.79 \pm 14.81) \times 10^{-1}$
5(1)	$(4.21 \pm 0.06) \times 10^{-1}$	$(5.25 \pm 0.07) \times 10^{-1}$	$(3.57 \pm 0.11) \times 10^{-1}$	$(1.90 \pm 0.56) \times 10^{-1}$	$(1.57 \pm 0.12) \times 10^{-1}$	$(5.13 \pm 53.36) \times 10^{-2}$
7(1)	$(3.04 \pm 0.04) \times 10^{-1}$	$(3.80 \pm 0.05) \times 10^{-1}$	$(2.50 \pm 0.10) \times 10^{-1}$	$(1.23 \pm 0.44) \times 10^{-1}$	$(7.41 \pm 0.69) \times 10^{-2}$	$(3.25 \pm 34.84) \times 10^{-2}$
9(1)	$(2.24 \pm 0.03) \times 10^{-1}$	$(2.60 \pm 0.04) \times 10^{-1}$	$(1.71 \pm 0.03) \times 10^{-1}$	$(6.84 \pm 1.80) \times 10^{-2}$	$(4.53 \pm 0.25) \times 10^{-2}$	$(1.87 \pm 19.03) \times 10^{-2}$
11(1)	$(1.68 \pm 0.03) \times 10^{-1}$	$(1.94 \pm 0.03) \times 10^{-1}$	$(1.24 \pm 0.02) \times 10^{-1}$	$(4.72 \pm 0.90) \times 10^{-2}$	$(2.84 \pm 0.13) \times 10^{-2}$	$(1.03 \pm 8.21) \times 10^{-2}$
13(1)	$(1.26 \pm 0.02) \times 10^{-1}$	$(1.42 \pm 0.02) \times 10^{-1}$	$(8.87 \pm 0.15) \times 10^{-2}$	$(2.96 \pm 0.44) \times 10^{-2}$	$(1.82 \pm 0.07) \times 10^{-2}$	$(9.95 \pm 55.65) \times 10^{-3}$
15(1)	$(9.12 \pm 0.19) \times 10^{-2}$	$(1.14 \pm 0.02) \times 10^{-1}$	$(6.36 \pm 0.11) \times 10^{-2}$	$(2.15 \pm 0.25) \times 10^{-2}$	$(1.13 \pm 0.04) \times 10^{-2}$	$(5.15 \pm 23.77) \times 10^{-3}$
17(1)	$(7.70 \pm 0.14) \times 10^{-2}$	$(8.21 \pm 0.12) \times 10^{-2}$	$(4.81 \pm 0.08) \times 10^{-2}$	$(1.40 \pm 0.13) \times 10^{-2}$	$(7.71 \pm 0.25) \times 10^{-3}$	$(5.74 \pm 21.01) \times 10^{-3}$
21(1)	$(4.29 \pm 0.06) \times 10^{-2}$	$(4.76 \pm 0.09) \times 10^{-2}$	$(2.46 \pm 0.04) \times 10^{-2}$	$(7.25 \pm 0.50) \times 10^{-3}$	$(3.03 \pm 0.13) \times 10^{-3}$	$(1.94 \pm 4.83) \times 10^{-3}$
23(1)	$(3.09 \pm 0.04) \times 10^{-2}$	$(2.81 \pm 0.07) \times 10^{-2}$	$(1.52 \pm 0.04) \times 10^{-2}$	$(3.98 \pm 0.24) \times 10^{-3}$	$(1.29 \pm 0.10) \times 10^{-3}$	$(1.80 \pm 3.96) \times 10^{-3}$
25(1)	$(2.21 \pm 0.04) \times 10^{-2}$	$(2.09 \pm 0.06) \times 10^{-2}$	$(1.06 \pm 0.03) \times 10^{-2}$	$(2.84 \pm 0.20) \times 10^{-3}$	$(1.05 \pm 0.08) \times 10^{-3}$	$(9.22 \pm 14.47) \times 10^{-4}$
27(1)	$(1.76 \pm 0.04) \times 10^{-2}$	$(1.42 \pm 0.06) \times 10^{-2}$	$(7.77 \pm 0.30) \times 10^{-3}$	$(1.94 \pm 0.15) \times 10^{-3}$	$(6.57 \pm 1.01) \times 10^{-4}$	$(8.50 \pm 11.15) \times 10^{-4}$
29(1)	$(1.26 \pm 0.03) \times 10^{-2}$	$(1.12 \pm 0.05) \times 10^{-2}$	$(5.40 \pm 0.22) \times 10^{-3}$	$(1.23 \pm 0.12) \times 10^{-3}$	$(5.11 \pm 1.17) \times 10^{-4}$	$(4.25 \pm 4.06) \times 10^{-4}$
31(1)	$(1.08 \pm 0.05) \times 10^{-2}$	$(8.23 \pm 0.87) \times 10^{-3}$	$(3.97 \pm 0.44) \times 10^{-3}$	$(9.42 \pm 3.41) \times 10^{-4}$	$(2.80 \pm 2.11) \times 10^{-4}$	$(4.43 \pm 10.94) \times 10^{-4}$
33(1)	$(7.91 \pm 0.72) \times 10^{-3}$	$(6.58 \pm 1.26) \times 10^{-3}$	$(3.02 \pm 0.46) \times 10^{-3}$	$(6.63 \pm 5.27) \times 10^{-4}$	$(2.64 \pm 4.16) \times 10^{-4}$	$(2.00 \pm 6.18) \times 10^{-4}$
35(1)	$(7.11 \pm 0.87) \times 10^{-3}$	$(5.01 \pm 1.77) \times 10^{-3}$	$(2.39 \pm 0.84) \times 10^{-3}$	$(5.24 \pm 15.95) \times 10^{-4}$	$(1.41 \pm 14.65) \times 10^{-4}$	$(2.29 \pm 1.87) \times 10^{-4}$
39(1)	$(4.07 \pm 1.84) \times 10^{-3}$	$(3.16 \pm 2.34) \times 10^{-3}$	$(1.23 \pm 3.72) \times 10^{-3}$	$(2.65 \pm 16.04) \times 10^{-4}$	$(9.27 \pm 223.44) \times 10^{-5}$	$(6.25 \pm 0.81) \times 10^{-5}$

θ (deg)	^{10}B $d\sigma/d\Omega$ (b sr^{-1})	^{11}B $d\sigma/d\Omega$ (b sr^{-1})	^{10}C $d\sigma/d\Omega$ (b sr^{-1})	^{11}C $d\sigma/d\Omega$ (b sr^{-1})	^{12}C $d\sigma/d\Omega$ (b sr^{-1})
3(1)	(1.61 ± 0.10)	(1.97 ± 0.02)	(1.49 ± 0.19)	(2.54 ± 0.94)	$(8.91 \pm 0.12) \times 10^{-3}$
5(1)	$(5.00 \pm 0.56) \times 10^{-1}$	$(8.29 \pm 0.18) \times 10^{-1}$	$(1.91 \pm 0.87) \times 10^{-1}$	(2.20 ± 1.61)	$(8.18 \pm 0.11) \times 10^{-3}$
7(1)	$(3.00 \pm 0.39) \times 10^{-1}$	$(3.44 \pm 0.13) \times 10^{-1}$	$(7.24 \pm 3.01) \times 10^{-2}$	$(6.66 \pm 4.09) \times 10^{-1}$	$(5.36 \pm 0.11) \times 10^{-3}$
9(1)	$(1.61 \pm 0.15) \times 10^{-1}$	$(1.71 \pm 0.02) \times 10^{-1}$	$(4.55 \pm 0.08) \times 10^{-2}$	$(2.85 \pm 0.05) \times 10^{-1}$	$(6.79 \pm 0.17) \times 10^{-3}$
11(1)	$(1.04 \pm 0.10) \times 10^{-1}$	$(9.46 \pm 0.13) \times 10^{-2}$	$(2.01 \pm 0.03) \times 10^{-2}$	$(1.23 \pm 0.02) \times 10^{-1}$	$(3.52 \pm 0.14) \times 10^{-3}$
13(1)	$(6.11 \pm 0.81) \times 10^{-2}$	$(5.35 \pm 0.07) \times 10^{-2}$	$(1.39 \pm 0.02) \times 10^{-2}$	$(6.71 \pm 0.17) \times 10^{-2}$	$(2.26 \pm 0.12) \times 10^{-3}$
15(1)	$(4.22 \pm 0.71) \times 10^{-2}$	$(3.08 \pm 0.05) \times 10^{-2}$	$(7.47 \pm 0.16) \times 10^{-3}$	$(3.03 \pm 0.08) \times 10^{-2}$	$(2.26 \pm 0.15) \times 10^{-3}$
17(1)	$(2.56 \pm 0.53) \times 10^{-2}$	$(1.80 \pm 0.03) \times 10^{-2}$	$(5.12 \pm 0.12) \times 10^{-3}$	$(1.56 \pm 0.06) \times 10^{-2}$	$(1.40 \pm 0.12) \times 10^{-3}$
21(1)	$(1.13 \pm 0.38) \times 10^{-2}$	$(6.22 \pm 0.22) \times 10^{-3}$	$(1.82 \pm 0.08) \times 10^{-3}$	$(4.41 \pm 0.15) \times 10^{-3}$	$(1.01 \pm 0.14) \times 10^{-3}$
23(1)	$(5.48 \pm 2.41) \times 10^{-3}$	$(2.99 \pm 0.19) \times 10^{-3}$	$(9.06 \pm 0.15) \times 10^{-4}$	$(1.89 \pm 0.03) \times 10^{-3}$	$(4.78 \pm 0.86) \times 10^{-4}$
25(1)	$(3.34 \pm 1.91) \times 10^{-3}$	$(1.88 \pm 0.25) \times 10^{-3}$	$(4.99 \pm 0.31) \times 10^{-4}$	$(1.07 \pm 0.03) \times 10^{-3}$	$(4.06 \pm 1.08) \times 10^{-4}$
27(1)	$(2.22 \pm 1.83) \times 10^{-3}$	$(1.08 \pm 0.32) \times 10^{-3}$	$(4.14 \pm 0.18) \times 10^{-4}$	$(6.31 \pm 1.37) \times 10^{-4}$	$(1.78 \pm 0.44) \times 10^{-4}$
29(1)	$(1.40 \pm 1.52) \times 10^{-3}$	$(7.31 \pm 7.94) \times 10^{-4}$	$(1.85 \pm 0.06) \times 10^{-4}$	$(2.89 \pm 3.76) \times 10^{-4}$	$(1.77 \pm 0.48) \times 10^{-4}$
31(1)	$(9.91 \pm 24.34) \times 10^{-4}$	$(4.20 \pm 28.41) \times 10^{-4}$	$(1.29 \pm 5.31) \times 10^{-4}$	$(2.02 \pm 25.73) \times 10^{-4}$	$(8.91 \pm 3.74) \times 10^{-5}$
33(1)	$(6.42 \pm 56.88) \times 10^{-4}$	$(3.58 \pm 90.84) \times 10^{-4}$	$(9.05 \pm 19.22) \times 10^{-5}$	$(1.34 \pm 64.27) \times 10^{-4}$	$(6.26 \pm 2.46) \times 10^{-5}$
35(1)	$(4.58 \pm 348.49) \times 10^{-4}$	$(1.65 \pm 0.13) \times 10^{-4}$	$(6.25 \pm 0.81) \times 10^{-5}$	$(8.02 \pm 0.92) \times 10^{-5}$	$(3.23 \pm 2.13) \times 10^{-5}$
39(1)	$(2.12 \pm 0.15) \times 10^{-4}$	$(8.64 \pm 0.96) \times 10^{-5}$	$(2.19 \pm 0.48) \times 10^{-5}$	$(3.54 \pm 0.61) \times 10^{-5}$	$(1.25 \pm 1.86) \times 10^{-5}$

APPENDIX E: DIFFERENTIAL CROSS SECTIONS FOR THE TITANIUM TARGET

TABLE VIII. ^{12}C fragmentation cross sections for the titanium target at different angles.

θ (deg)	^{1}H $d\sigma/d\Omega$ (b sr^{-1})	^{2}H $d\sigma/d\Omega$ (b sr^{-1})	^{3}H $d\sigma/d\Omega$ (b sr^{-1})	^{3}He $d\sigma/d\Omega$ (b sr^{-1})	^{4}He $d\sigma/d\Omega$ (b sr^{-1})	^{6}He $d\sigma/d\Omega$ (b sr^{-1})
3(1)	(2.73 ± 0.04)	(1.58 ± 0.02)	(1.04 ± 0.01)	$(8.44 \pm 0.35) \times 10^{-1}$	$(1.49 \pm 0.02) \times 10^{1}$	$(9.05 \pm 1.47) \times 10^{-2}$
5(1)	(1.86 ± 0.14)	(1.21 ± 0.05)	$(8.02 \pm 0.19) \times 10^{-1}$	$(7.22 \pm 0.77) \times 10^{-1}$	(9.28 ± 0.30)	$(5.96 \pm 4.39) \times 10^{-2}$
7(1)	(1.92 ± 0.14)	(1.20 ± 0.05)	$(7.75 \pm 0.14) \times 10^{-1}$	$(7.06 \pm 0.79) \times 10^{-1}$	(6.89 ± 0.26)	$(5.33 \pm 4.32) \times 10^{-2}$
9(1)	(1.70 ± 0.03)	(1.09 ± 0.01)	$(6.98 \pm 0.28) \times 10^{-1}$	$(5.72 \pm 0.71) \times 10^{-1}$	(5.21 ± 0.20)	$(3.26 \pm 2.93) \times 10^{-2}$
13(1)	(1.38 ± 0.02)	$(8.82 \pm 0.12) \times 10^{-1}$	$(5.26 \pm 0.21) \times 10^{-1}$	$(3.96 \pm 0.48) \times 10^{-1}$	(2.89 ± 0.11)	$(2.02 \pm 2.12) \times 10^{-2}$
15(1)	(1.31 ± 0.02)	$(7.84 \pm 0.11) \times 10^{-1}$	$(4.57 \pm 0.18) \times 10^{-1}$	$(3.37 \pm 0.38) \times 10^{-1}$	(2.18 ± 0.08)	$(1.83 \pm 1.89) \times 10^{-2}$
17(1)	(1.11 ± 0.02)	$(7.06 \pm 0.10) \times 10^{-1}$	$(3.67 \pm 0.14) \times 10^{-1}$	$(2.61 \pm 0.26) \times 10^{-1}$	(1.74 ± 0.05)	$(1.26 \pm 1.25) \times 10^{-2}$
21(1)	$(9.12 \pm 0.11) \times 10^{-1}$	$(5.34 \pm 0.05) \times 10^{-1}$	$(2.92 \pm 0.07) \times 10^{-1}$	$(1.90 \pm 0.11) \times 10^{-1}$	(1.11 ± 0.02)	$(9.46 \pm 5.51) \times 10^{-3}$
23(1)	$(8.10 \pm 0.15) \times 10^{-1}$	$(4.61 \pm 0.07) \times 10^{-1}$	$(2.55 \pm 0.08) \times 10^{-1}$	$(1.58 \pm 0.11) \times 10^{-1}$	$(8.90 \pm 0.17) \times 10^{-1}$	$(7.70 \pm 5.49) \times 10^{-3}$
25(1)	$(7.11 \pm 0.14) \times 10^{-1}$	$(4.08 \pm 0.06) \times 10^{-1}$	$(2.18 \pm 0.05) \times 10^{-1}$	$(1.32 \pm 0.08) \times 10^{-1}$	$(7.39 \pm 0.11) \times 10^{-1}$	$(6.05 \pm 3.56) \times 10^{-3}$
27(1)	$(6.68 \pm 0.13) \times 10^{-1}$	$(3.71 \pm 0.05) \times 10^{-1}$	$(1.94 \pm 0.04) \times 10^{-1}$	$(1.13 \pm 0.06) \times 10^{-1}$	$(6.31 \pm 0.08) \times 10^{-1}$	$(5.36 \pm 2.80) \times 10^{-3}$
31(1)	$(5.45 \pm 0.11) \times 10^{-1}$	$(2.86 \pm 0.05) \times 10^{-1}$	$(1.41 \pm 0.02) \times 10^{-1}$	$(7.67 \pm 0.41) \times 10^{-2}$	$(4.35 \pm 0.09) \times 10^{-1}$	$(3.38 \pm 1.65) \times 10^{-3}$
33(1)	$(4.66 \pm 0.10) \times 10^{-1}$	$(2.46 \pm 0.04) \times 10^{-1}$	$(1.17 \pm 0.02) \times 10^{-1}$	$(6.10 \pm 0.34) \times 10^{-2}$	$(3.54 \pm 0.10) \times 10^{-1}$	$(2.73 \pm 1.34) \times 10^{-3}$
35(1)	$(4.51 \pm 0.10) \times 10^{-1}$	$(2.15 \pm 0.04) \times 10^{-1}$	$(1.04 \pm 0.02) \times 10^{-1}$	$(5.12 \pm 0.33) \times 10^{-2}$	$(3.03 \pm 0.14) \times 10^{-1}$	$(2.27 \pm 1.15) \times 10^{-3}$
39(1)	$(3.55 \pm 0.06) \times 10^{-1}$	$(1.70 \pm 0.03) \times 10^{-1}$	$(7.37 \pm 0.14) \times 10^{-2}$	$(3.44 \pm 0.22) \times 10^{-2}$	$(2.12 \pm 0.13) \times 10^{-1}$	$(1.47 \pm 0.71) \times 10^{-3}$

θ (deg)	^{6}Li $d\sigma/d\Omega$ (b sr^{-1})	^{7}Li $d\sigma/d\Omega$ (b sr^{-1})	^{7}Be $d\sigma/d\Omega$ (b sr^{-1})	^{9}Be $d\sigma/d\Omega$ (b sr^{-1})	^{10}Be $d\sigma/d\Omega$ (b sr^{-1})	^{8}B $d\sigma/d\Omega$ (b sr^{-1})
3(1)	$(7.91 \pm 0.07) \times 10^{-1}$	$(9.29 \pm 0.10) \times 10^{-1}$	$(5.93 \pm 0.19) \times 10^{-1}$	$(6.14 \pm 0.61) \times 10^{-1}$	$(2.94 \pm 0.17) \times 10^{-1}$	$(2.26 \pm 18.77) \times 10^{-1}$
5(1)	$(4.57 \pm 0.06) \times 10^{-1}$	$(6.09 \pm 0.09) \times 10^{-1}$	$(3.68 \pm 0.11) \times 10^{-1}$	$(2.29 \pm 0.67) \times 10^{-1}$	$(1.89 \pm 0.14) \times 10^{-1}$	$(5.46 \pm 56.90) \times 10^{-2}$
7(1)	$(3.33 \pm 0.05) \times 10^{-1}$	$(4.31 \pm 0.06) \times 10^{-1}$	$(2.57 \pm 0.09) \times 10^{-1}$	$(1.35 \pm 0.48) \times 10^{-1}$	$(9.06 \pm 0.81) \times 10^{-2}$	$(3.24 \pm 34.77) \times 10^{-2}$
9(1)	$(2.45 \pm 0.04) \times 10^{-1}$	$(2.95 \pm 0.05) \times 10^{-1}$	$(1.71 \pm 0.03) \times 10^{-1}$	$(7.67 \pm 2.01) \times 10^{-2}$	$(5.02 \pm 0.28) \times 10^{-2}$	$(1.77 \pm 18.04) \times 10^{-2}$
13(1)	$(1.36 \pm 0.02) \times 10^{-1}$	$(1.52 \pm 0.02) \times 10^{-1}$	$(8.48 \pm 0.15) \times 10^{-2}$	$(3.29 \pm 0.50) \times 10^{-2}$	$(1.95 \pm 0.08) \times 10^{-2}$	$(8.79 \pm 49.25) \times 10^{-3}$
15(1)	$(1.01 \pm 0.02) \times 10^{-1}$	$(1.17 \pm 0.02) \times 10^{-1}$	$(5.94 \pm 0.11) \times 10^{-2}$	$(2.28 \pm 0.27) \times 10^{-2}$	$(1.28 \pm 0.05) \times 10^{-2}$	$(4.08 \pm 18.89) \times 10^{-3}$
17(1)	$(8.04 \pm 0.13) \times 10^{-2}$	$(8.15 \pm 0.13) \times 10^{-2}$	$(4.22 \pm 0.08) \times 10^{-2}$	$(1.56 \pm 0.15) \times 10^{-2}$	$(8.95 \pm 0.33) \times 10^{-3}$	$(4.48 \pm 16.45) \times 10^{-3}$
21(1)	$(4.87 \pm 0.05) \times 10^{-2}$	$(5.23 \pm 0.07) \times 10^{-2}$	$(2.38 \pm 0.04) \times 10^{-2}$	$(8.81 \pm 0.46) \times 10^{-3}$	$(4.11 \pm 0.15) \times 10^{-3}$	$(1.63 \pm 2.89) \times 10^{-3}$
23(1)	$(3.88 \pm 0.05) \times 10^{-2}$	$(3.84 \pm 0.10) \times 10^{-2}$	$(1.79 \pm 0.05) \times 10^{-2}$	$(6.32 \pm 0.38) \times 10^{-3}$	$(2.41 \pm 0.17) \times 10^{-3}$	$(2.29 \pm 5.04) \times 10^{-3}$
25(1)	$(3.03 \pm 0.05) \times 10^{-2}$	$(3.20 \pm 0.09) \times 10^{-2}$	$(1.32 \pm 0.04) \times 10^{-2}$	$(4.67 \pm 0.31) \times 10^{-3}$	$(2.05 \pm 0.14) \times 10^{-3}$	$(1.30 \pm 2.03) \times 10^{-3}$
27(1)	$(2.55 \pm 0.06) \times 10^{-2}$	$(2.38 \pm 0.10) \times 10^{-2}$	$(1.02 \pm 0.04) \times 10^{-2}$	$(3.65 \pm 0.24) \times 10^{-3}$	$(1.28 \pm 0.18) \times 10^{-3}$	$(1.24 \pm 1.62) \times 10^{-3}$
31(1)	$(1.60 \pm 0.07) \times 10^{-2}$	$(1.39 \pm 0.15) \times 10^{-2}$	$(5.64 \pm 0.64) \times 10^{-3}$	$(2.02 \pm 0.73) \times 10^{-3}$	$(6.68 \pm 4.99) \times 10^{-4}$	$(6.28 \pm 15.59) \times 10^{-4}$
33(1)	$(1.16 \pm 0.11) \times 10^{-2}$	$(1.09 \pm 0.21) \times 10^{-2}$	$(4.15 \pm 0.64) \times 10^{-3}$	$(1.35 \pm 1.07) \times 10^{-3}$	$(5.73 \pm 8.99) \times 10^{-4}$	$(3.43 \pm 10.59) \times 10^{-4}$
35(1)	$(9.79 \pm 1.25) \times 10^{-3}$	$(8.29 \pm 2.95) \times 10^{-3}$	$(2.92 \pm 1.06) \times 10^{-3}$	$(1.02 \pm 3.11) \times 10^{-3}$	$(3.80 \pm 39.54) \times 10^{-4}$	$(3.50 \pm 2.93) \times 10^{-4}$
39(1)	$(5.70 \pm 1.85) \times 10^{-3}$	$(5.09 \pm 2.69) \times 10^{-3}$	$(1.71 \pm 3.69) \times 10^{-3}$	$(5.70 \pm 24.50) \times 10^{-4}$	$(1.90 \pm 32.61) \times 10^{-4}$	$(1.45 \pm 0.15) \times 10^{-4}$

θ (deg)	^{10}B $d\sigma/d\Omega$ (b sr^{-1})	^{11}B $d\sigma/d\Omega$ (b sr^{-1})	^{10}C $d\sigma/d\Omega$ (b sr^{-1})	^{11}C $d\sigma/d\Omega$ (b sr^{-1})	^{12}C $d\sigma/d\Omega$ (b sr^{-1})
3(1)	(1.95 ± 0.13)	(2.39 ± 0.02)	(3.09 ± 0.33)	(3.98 ± 1.65)	$(1.50 \pm 0.02) \times 10^{-2}$
5(1)	$(5.67 \pm 0.63) \times 10^{-1}$	$(9.26 \pm 0.19) \times 10^{-1}$	$(2.50 \pm 1.22) \times 10^{-1}$	(3.25 ± 2.59)	$(1.11 \pm 0.02) \times 10^{-2}$
7(1)	$(2.97 \pm 0.37) \times 10^{-1}$	$(3.64 \pm 0.12) \times 10^{-1}$	$(6.49 \pm 2.91) \times 10^{-2}$	$(5.87 \pm 3.74) \times 10^{-1}$	$(4.57 \pm 0.10) \times 10^{-3}$
9(1)	$(1.59 \pm 0.15) \times 10^{-1}$	$(1.65 \pm 0.02) \times 10^{-1}$	$(4.46 \pm 0.07) \times 10^{-2}$	$(2.73 \pm 0.05) \times 10^{-1}$	$(1.24 \pm 0.03) \times 10^{-2}$
13(1)	$(5.62 \pm 0.76) \times 10^{-2}$	$(4.76 \pm 0.07) \times 10^{-2}$	$(1.24 \pm 0.02) \times 10^{-2}$	$(7.53 \pm 0.18) \times 10^{-2}$	$(2.41 \pm 0.15) \times 10^{-3}$
15(1)	$(3.72 \pm 0.63) \times 10^{-2}$	$(2.94 \pm 0.05) \times 10^{-2}$	$(5.60 \pm 0.09) \times 10^{-3}$	$(2.38 \pm 0.06) \times 10^{-2}$	$(2.27 \pm 0.17) \times 10^{-3}$
17(1)	$(2.40 \pm 0.51) \times 10^{-2}$	$(1.71 \pm 0.04) \times 10^{-2}$	$(4.17 \pm 0.07) \times 10^{-3}$	$(1.32 \pm 0.04) \times 10^{-2}$	$(1.15 \pm 0.13) \times 10^{-3}$
21(1)	$(1.17 \pm 0.28) \times 10^{-2}$	$(7.67 \pm 0.23) \times 10^{-3}$	$(1.73 \pm 0.04) \times 10^{-3}$	$(4.51 \pm 0.08) \times 10^{-3}$	$(1.12 \pm 0.12) \times 10^{-3}$
23(1)	$(7.20 \pm 3.18) \times 10^{-3}$	$(4.56 \pm 0.29) \times 10^{-3}$	$(1.09 \pm 0.01) \times 10^{-3}$	$(2.71 \pm 0.04) \times 10^{-3}$	$(5.41 \pm 1.04) \times 10^{-4}$
25(1)	$(5.03 \pm 2.85) \times 10^{-3}$	$(3.56 \pm 0.44) \times 10^{-3}$	$(7.32 \pm 0.38) \times 10^{-4}$	$(1.74 \pm 0.03) \times 10^{-3}$	$(5.22 \pm 1.34) \times 10^{-4}$
27(1)	$(3.94 \pm 3.22) \times 10^{-3}$	$(2.04 \pm 0.57) \times 10^{-3}$	$(5.68 \pm 0.19) \times 10^{-4}$	$(1.03 \pm 0.21) \times 10^{-3}$	$(4.11 \pm 0.86) \times 10^{-4}$
31(1)	$(1.88 \pm 4.62) \times 10^{-3}$	$(9.11 \pm 61.53) \times 10^{-4}$	$(2.62 \pm 10.73) \times 10^{-4}$	$(4.71 \pm 60.04) \times 10^{-4}$	$(1.86 \pm 0.77) \times 10^{-4}$
33(1)	$(1.23 \pm 10.91) \times 10^{-3}$	$(6.96 \pm 176.85) \times 10^{-4}$	$(1.28 \pm 2.75) \times 10^{-4}$	$(2.09 \pm 100.77) \times 10^{-4}$	$(1.34 \pm 0.51) \times 10^{-4}$
35(1)	$(1.00 \pm 76.25) \times 10^{-3}$	$(3.93 \pm 0.33) \times 10^{-4}$	$(1.26 \pm 0.18) \times 10^{-4}$	$(1.60 \pm 0.21) \times 10^{-4}$	$(1.02 \pm 0.65) \times 10^{-4}$
39(1)	$(4.18 \pm 0.25) \times 10^{-4}$	$(2.11 \pm 0.18) \times 10^{-4}$	$(4.31 \pm 0.79) \times 10^{-5}$	$(5.49 \pm 0.89) \times 10^{-5}$	$(3.88 \pm 4.04) \times 10^{-5}$

[1] D. Schardt, T. Elsässer, and D. Schulz-Ertner, Rev. Mod. Phys. **82**, 383 (2010).

[2] A. S. Goldhaber and H. H. Heckman, Annu. Rev. Nucl. Sci. **28**, 161 (1978).

[3] E. Haettner, H. Iwase, and D. Schardt, Radiat. Prot. Dosim. **122**, 485 (2006).

[4] M. De Napoli *et al.*, Phys. Med. Biol. **57**, 7651 (2012).

[5] T. T. Böhlen, F. Cerutti, M. Dosanjh, A. Ferrari, I. Gudowska, A. Mairani, and J. M. Quesada, Phys. Med. Biol. **55**, 5833 (2010).

[6] B. Braunn *et al.*, J. Phys: Conf. Series **420**, 012163 (2013).

[7] J. Dudouet, D. Cussol, D. Durand, and M. Labalme, Phys. Rev. C **89**, 054616 (2014).

[8] N. Matsufuji, A. Fukumura, M. Komori, T. Kanai, and T. Kohno, Phys. Med. Biol. **48**, 1605 (2003).

[9] N. Matsufuji *et al.*, Phys. Med. Biol **50**, 3393 (2005).

[10] G. De Lellis *et al.*, Nucl. Phys. A **853**, 124 (2011).

[11] D. Schardt *et al.*, Adv. Space Res. **17**, 87 (1996).

[12] E. Haetnner, MsC thesis, 2005.

[13] K. Gunzert-Marx, H. Iwase, D. Schardt, and R. S. Simon, New J. Phys. **10**, 075003 (2008).

[14] E. Haetnner, H. Iwase, M. Krmer, G. Kraft, and D. Schardt, Phys. Med. Biol. **58**, 8265 (2013).

[15] B. Braunn *et al.*, Nucl. Instrum. Methods Phys. Res. B **269**, 2676 (2011).

[16] J. Dudouet, D. Juliani, M. Labalme, D. Cussol, J. C. Angelique, B. Braunn, J. Colin, C. Finck, J. M. Fontbonne, H. Guerin, P. Henriquet, J. Krimmer, M. Rousseau, M.G. Saint-Laurent, and S. Salvador, Phys. Rev. C **88**, 024606 (2013).

[17] J. Dudouet, M. Labalme, D. Cussol, C. Finck, R. Rescigno, M. Rousseau, S. Salvador, and M. Vanstalle, Phys. Rev. C **89**, 064615 (2014).

[18] T. Ogawa, S. Hashimoto, T. Sato, and K. Niita, EPJ Web Conf. **117**, 03011 (2016).

[19] T. Sato *et al.*, J. Nucl. Sci. Technol. **50**, 913 (2013).

[20] S. G. Mashnik, L. M. Kerby, K. K. Gudima, and A. J. Sierk, EPJ Web Conf. **66**, 03059 (2014).

[21] G. W. McKinney, F. B. Brown, H. G. Hughes, M. R. James, R. L. Martz, G. E. McMath, and T. A. Wilcox, *IEEE 2014 Nuclear Science Symposium and Medical Imaging Conference* (IEEE, Seattle, 2014).

[22] D. Mancusi, A. Boudard, J. Carbonell, J. Cugnon, J. C. David, and S. Leray, Phys. Rev. C **90**, 054602 (2015).

[23] S. Agostinelli *et al.*, Nucl. Instrum. Methods Phys. Res. A **506**, 250 (2003).

[24] J. Dudouet *et al.*, Nucl. Instrum. Methods Phys. Res. A **715**, 98 (2013).

[25] FASTER Collaboration, http://faster.in2p3.fr/.

[26] J. Frankland *et al.*, Kaliveda data analysis framework http://indra.in2p3.fr/kalivedadoc.

[27] K. Niita *et al.*, JAERIData/Code 99-042, 31, 1999.

[28] J. Dudouet, Ph.D. thesis, Université de Caen, 2014.